PHILOSOPHICAL TRANSACTIONS OF THE ROYAL SOCIETY A MATHEMATICAL, PHYSICAL & ENGINEERING SCIENCES

Atmospheric Angular Momentum Forecasts as Novel Tests of Global Numerical Weather Prediction Models

M. J. Bell, R. Hide and G. Sakellarides

Phil. Trans. R. Soc. Lond. A 1991 **334**, 55-92
doi: 10.1098/rsta.1991.0003

Atmospheric angular momentum forecasts as novel tests of global numerical weather prediction models

By M. J. Bell[1], R. Hide[1]† and G. Sakellarides[2]‡

[1] *Meteorological Office, Bracknell, Berkshire RG12 2SZ, U.K.*

[2] *European Centre for Medium-Range Weather Forecasts, Shinfield, Berkshire RG2 9AX, U.K.*

Contents

The global circulation of the terrestrial atmosphere exhibits fluctuations of considerable amplitude in all three components of its total angular momentum on interannual, seasonal and shorter timescales. The fluctuations must be intimately linked with nonlinear barotropic and baroclinic energetic conversion processes throughout the whole atmosphere and it is advocated that studies of routinely produced determinations of atmospheric angular momentum (AAM) changes be incorporated into systematic diagnostic investigations of large-scale atmospheric flows. AAM fluctuations are generated by dynamical interactions between the atmosphere and the underlying planet. These excite tiny but measurable compensating fluctuations in the rotation vector of the massive solid Earth, thereby ensuring conservation of the angular momentum of the whole system. Forecasts and analyses of changes in AAM from the output of a global numerical weather prediction (GNWP) model constitute a stringent test of the model. Successful forecasts of the axial component of AAM, and hence of irregular non-tidal components of short-term changes in the Earth's rotation, would find practical applications in various areas of astronomy and geodesy, such as spacecraft navigation. Reported in this paper are the main findings of intercomparisons of analyses and forecasts of changes in all three components of AAM obtained from the operational GNWP models at the United Kingdom Meteorological Office (UKMO) and the European Centre for Medium-

† Present address: The Robert Hooke Institute, Old Observatory, Clarendon Laboratory, Parks Road, Oxford OX1 3PU, U.K.

‡ Present address: The Hellenic National Meteorological Service, P.O. Box 603 (Hellenikon), Athens, Greece.

Phil. Trans. R. Soc. Lond. A (1991) **334**, 55–92 55

Printed in Great Britain

Range Weather Forecasts (ECMWF), over the period covering the two years 1987 and 1988. Included in the results obtained is the finding that useful forecasts of changes in the axial component of AAM can be made out to 5 days and even slightly longer.

1. Introduction

The absolute angular momentum of the atmosphere H_i (say) can be written as the sum of two terms

$$H_i \equiv H_i^{\mathrm{p}} + H_i^{\mathrm{w}}, \tag{1.1}$$

where

$$H_i^{\mathrm{p}} \equiv \iiint \rho \epsilon_{ijk} x_j \epsilon_{klm} \omega_l x_m \,\mathrm{d(volume)} \tag{1.2a}$$

and

$$H_i^{\mathrm{w}} \equiv \iiint \rho \epsilon_{ijk} x_j u_k \,\mathrm{d(volume)}, \tag{1.2b}$$

respectively the 'matter' and the 'wind' contributions to H_i (see, for example, Barnes *et al.* 1983, hereafter cited as BHWW). Here $\rho(x_i, t)$ and $u_k(x_i, t)$ denote the mass density and wind velocity respectively at a general point x_i, $i = 1, 2, 3$, within the atmosphere, over the whole of which the volume integral is taken. The usual summation convention is used for repeated suffixes and ϵ_{ijk} is the alternating tensor with values 0 or ± 1. The frame of reference used has its origin at the centre of mass of the whole Earth (solid inner core, liquid outer core, 'solid Earth', hydrosphere, atmosphere) and is aligned with the principal axes of inertia of the 'solid Earth' (mantle, crust and cryosphere), see figure 1. With respect to an inertial frame, the body-fixed frame of reference rotates with angular velocity $\omega_i(t)$, $i = 1, 2, 3$.

All components of H_i vary with time as a consequence of dynamical interactions between the atmosphere and the underlying planet. These interactions (and other

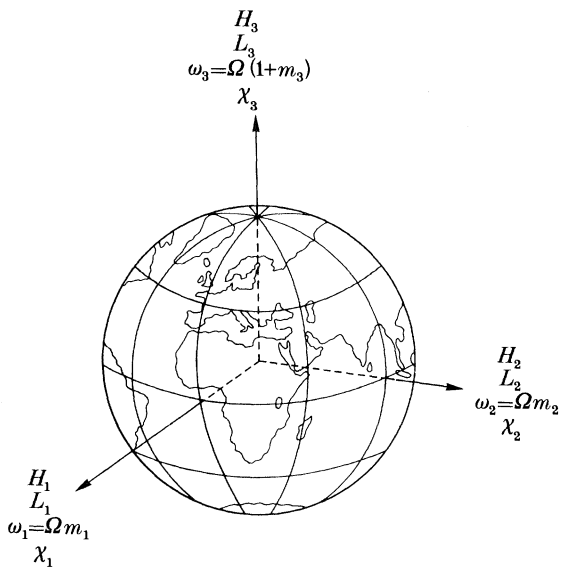

Figure 1. Illustrating the components of the vectors H_i, L_i, m_i and ω_i and the dimensionless pseudo-vector χ_i (see equations (1.1) to (1.4) and (2.1) to (2.6)).

agencies, see Appendix A), produce measurable fluctuations in ω_i, and it is customary to write

$$\omega_i(t) \equiv (\omega_1(t)_1\, \omega_2(t), \omega_3(t)) \equiv \Omega(m_1(t), m_2(t), 1+m_3(t)), \tag{1.3}$$

where $\Omega = 0.7292115 \times 10^{-4}$ radians per sidereal second is the mean angular speed of rotation of the solid Earth in recent times (see figure 1). Over timescales that are short compared with those of geological processes, the magnitudes of the dimensionless quantities $m_1(t), m_2(t)$ and $m_3(t)$ are all very much less than unity, so that for the purpose of determining H_i from meteorological data using equations (1.1) and (1.2), it is sufficient to set $m_i = 0$, so that $\omega_i = (0, 0, \Omega)$.

The non-zero meteorological contributions to $m_i(t)$ are, of course, important in the study of fluctuations in the Earth's rotation. If L_i is the net torque acting on the Earth's atmosphere then

$$L_i = \mathrm{d}H_i/\mathrm{d}t = \dot{H}_i + \epsilon_{ijk}\, \omega_j\, H_k. \tag{1.4}$$

$\mathrm{d}H_i/\mathrm{d}t$ and $\dot{H}_i$ are the respective time rates of change of H_i with respect to an inertial frame and the rotating frame, and when $\omega_i = (0, 0, \Omega)$ we have

$$L_1 = \dot{H}_1 - \Omega H_2, \quad L_2 = \dot{H}_2 + \Omega H_1, \quad L_3 = \dot{H}_3 \tag{1.5}$$

(see equations (1.1) and (1.2)). It is well known that L_i is hard to estimate directly from surface drag determinations, owing to the high degree of cancelling involved and other practical difficulties (see Wahr & Oort 1984; Swinbank 1985; Wolf & Smith 1987). But L_i can be determined indirectly with useful accuracy from wind observations at all levels within the atmosphere by using the expressions given by equation (1.5). Through the action of L_i, angular momentum is exchanged back and forth between the atmosphere and the underlying planet, the surface of which is subjected by the atmosphere to an applied torque equal to $-L_i$. Most of the angular momentum exchanged, which in magnitude can be a considerable fraction of that of H_i^{w} (see equation (1.2)), goes into the massive solid Earth, whose moment of inertia is some 10^6 times that of the atmosphere. This produces tiny but measurable changes in the length of the day,

$$\Lambda(t) = \Lambda_0/(1+m_3(t)), \quad \text{where} \quad \Lambda_0 \equiv 2\pi/\Omega, \tag{1.6a}$$

and movements of the poles of the instantaneous axis of rotation of the solid Earth relative to its axis of figure, as specified by the quantity

$$\boldsymbol{m}(t) \equiv m_1(t) + \mathrm{i} m_2(t), \tag{1.6b}$$

where $\mathrm{i} \equiv \sqrt{-1}$ (see equation (1.3)). Indeed, the largest torques acting on the solid Earth are generated by atmospheric motions, which produce changes in Λ of up to about 0.5×10^{-3} s in magnitude fluctuating irregularly on timescales as short as a few days (corresponding to changes in $|m_3|$ slightly less than about 10^{-8}) and displacements of the pole of rotation of several metres (corresponding to changes in $|\boldsymbol{m}|$ of about 10^{-6}).

The torque $-L_i$ is due to (*a*) tangential stresses in the turbulent boundary layers over the continents and oceans, and (*b*) normal stresses acting on continental orography and the Earth's equatorial bulge. Owing to the rigidity (albeit slightly imperfect) of the solid Earth, all three components of the 'continental' part of $-L_i$ are transmitted to the solid Earth directly and fully. The oceanic part of $-L_i$ gives rise to a dynamical response in the oceans which has not yet been fully investigated, but the case when the whole of the applied torque is assumed to be passed on by the

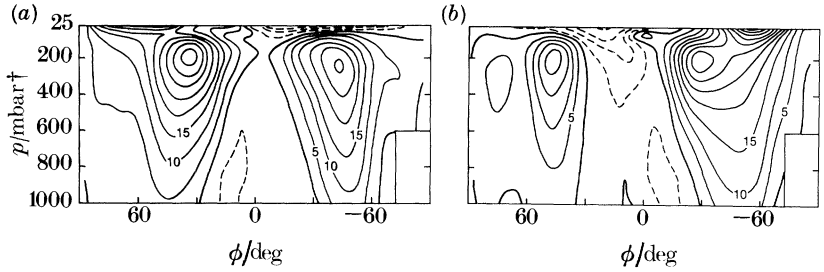

Figure 2. The (ϕ (latitude), p (pressure level)) distribution within the atmosphere of $\bar{u}(\phi, p)$ (m s^{-1}), the monthly-mean value of the average with respect to λ (longitude) of the eastward (westerly) component $u(\phi, \lambda, p, t)$ of the wind for (*a*) January 1988, and (*b*) July 1988. The data are based on ECMWF 'analyses' of routine meteorological observations.

oceans to the solid Earth virtually instantaneously (i.e. in no more than a few hours) can be taken as realistic for practical purposes, particularly when dealing with the axial component of $-L_i$ and the changes in A it produces. Thus, the oceans act as an intermediary in the angular momentum exchange process by transmitting the applied stresses in the atmospheric boundary layer over the oceans to the continental margins and ocean bottom. It will be important in this connection to examine oceanographic data, such as fluctuations in sea level at continental margins, that might elucidate the mechanisms involved (see, for example, Bongers & Wyrtki 1987; Carton & Wahr 1986; Mitchum & Lukas 1987; Nowlin & Klinck 1986; Spillane *et al.* 1987; Wyrtki 1985). It is a fortunate circumstance that, owing to the slowness and scales of ocean currents in comparison with atmospheric winds, in the budget of angular momentum between the solid Earth and its overlying fluid layers, the hydrosphere (in spite of its much greater moment of inertia than that of the atmosphere, by a factor of about 300) produces effects that can be neglected to a first approximation.

Global numerical weather prediction (GNWP) models are used at meteorological centres in several countries. The task of improving the performance of these models by identifying and correcting weaknesses in their formulation requires systematic work on soundly based diagnostic methods for testing model performance. In this paper we advocate the inclusion of atmospheric angular momentum (AAM) analyses and forecasts in such tests, for two main reasons. The first and most obvious is the unique opportunity it provides, in principle at least, for comparing on a clear-cut physical basis the output of a global quantity from the models with observations that are completely independent of meteorological data, namely those of short-term fluctuations of the rotation of the solid Earth (see Rosen *et al.* 1987*b*; Hide 1988, 1990; and Appendix A). Secondly, considerations of AAM fluctuations bear directly on fundamental aspects of the energetics of the global atmospheric circulation and cannot be separated from them (see, for example, Hide 1989; White 1989). In the absence of energy sources, the atmosphere would rotate with the solid Earth like a rigid body (i.e. $u_i = 0$ everywhere). This would be a state of minimum kinetic energy of the whole system for given total angular momentum (see Appendix B). Differential solar heating produces atmospheric winds, the kinetic energy of which derives from the available potential energy of the atmosphere (which is associated with gravity acting on the density field maintained by the heating) through the action of vertical motions. Angular momentum is thereby redistributed without any change occurring

† 1 bar = 10^5 Pa.

PHILOSOPHICAL TRANSACTIONS OF THE ROYAL SOCIETY A MATHEMATICAL, PHYSICAL & ENGINEERING SCIENCES

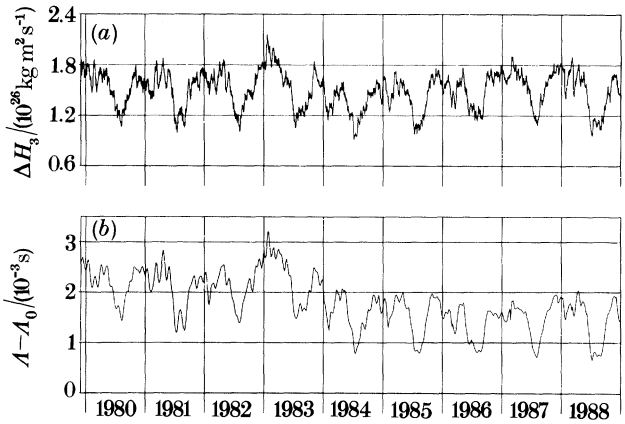

Figure 3. (*a*) Time series of $\Delta H_3(t)$, defined as the axial component of the angular momentum of the atmosphere (see equation (1.2)) minus the mean value of the matter term H_3^{p}, from 1 January 1980 to 31 December 1988. (*b*) The corresponding length of the day $\Lambda(t)$ (see equation (1.6*a*)) after periodic changes due to solid Earth tides have been removed. The ordinates are scaled so as to enable direct quantitative comparison (see equations (2.1), (2.3) and (1.6*a*)). There is good qualitative and quantitative agreement between the corresponding changes in χ_3 (proportional to H_3) and $-m_3$ (equal to $1-\Lambda_0/\Lambda$), on timescales less than about two years, which implies that short-term irregular changes in the length of the day can be accounted for in terms of angular momentum exchange between the atmosphere and the solid Earth, without having to invoke non-meteorological excitation on these timescales. The long-term trend in the difference between the upper and lower curves gives the 'decadal' change in the length of the day, which geophysicists consider to be due to torques applied to the solid Earth by the underlying liquid, metallic core (see text). (*a*) is based on ECMWF initialized analyses of routine meteorological observations, and (*b*) is based on Earth rotation observations supplied by the International Earth Rotation Service (IERS) (formerly Bureau International de l'Heure (BIH)). ($\Lambda_0 \equiv 86400$ sidereal seconds.)

in the total amount in the whole system (since solar heating produces no net torque). The largest contribution to the kinetic energy of the atmosphere associated with atmospheric winds is that made by the zonal 'super-rotation' at an average speed U (say) of about 10 m s^{-1}, namely $\frac{1}{2}MU^2$, where M is the total mass of the atmosphere (see figure 2). Observed fluctuations in the axial component of AAM (see figure 3*a*) amount to a considerable fraction of $MU\bar{R}$ in magnitude (where $\bar{R}$ is the mean radius of the solid Earth), and there are compensating fluctuations in the angular momentum of the solid Earth (see figure 3*b*). Concomitant fluctuations in the kinetic energy associated with the super-rotation, amount to a considerable fraction of $\frac{1}{2}MU^2$ (see Appendix B). By energy conservation arguments, the latter can only be produced by dynamical processes involving nonlinear interactions between the zonal wind field, the non-zonal wind field and the field of available potential energy in the atmosphere. Successful models of the global circulation of the atmosphere must represent these interactions correctly.

So far as direct applications of AAM forecasts are concerned, they could be used in astronomy and geodesy, including spacecraft navigation where, for example, fuel economy on the Galileo mission to the planet Jupiter, the Magellan mission to Venus and the planned Cassini mission to Saturn requires length-of-day (l.o.d.) forecasts out to about 5 d ahead. Organizations such as the International Earth Rotation Service (IERS) (see Appendix A) now make use of routine AAM analyses and forecasts in their practical operations.

In place of H_i it is convenient to use the dimensionless AAM functions χ_i defined in §2 (see equations (2.1)–(2.3)), where a brief account is also given of the GNWP models used at the UKMO and ECMWF in the determination of analyses and forecasts of χ_i. From the outputs of these models in 1987 and 1988, analyses and forecasts of all three components of χ_i have been produced. The axial component time series $\chi_3(t)$ is discussed in §3 and compared with length of day time series in §4. The equatorial components χ_1 and χ_2 are discussed in §5, and concluding remarks given in §6. Further discussion of agencies responsible for fluctuations in the Earth's rotation on all timescales is presented in Appendix A, and the torque acting on the Earth's equatorial bulge is considered in Appendix C.

2. Atmospheric angular momentum functions and global numerical weather prediction models

In the theory of the interactions between the atmosphere and underlying planet that give rise to fluctuations in H_i (see BHWW) the analysis is facilitated by using in place of H_i the dimensionless AAM functions χ_i, $i = 1, 2, 3$ (see figure 1), which are now calculated routinely at various meteorological centres. These are defined as follows:

$$\chi_i \equiv \chi_i^{\mathrm{p}} + \chi_i^{\mathrm{w}} = \int_{-\pi/2}^{\pi/2} \xi_i(\phi, t)\,\mathrm{d}\phi = \int_{-\pi/2}^{\pi/2} [\xi_i^{\mathrm{p}}(\phi, t) + \xi_i^{\mathrm{w}}(\phi, t)]\,\mathrm{d}\phi, \tag{2.1}$$

where

$$(\xi_1^{\mathrm{p}}, \xi_2^{\mathrm{p}}) \equiv \frac{-1.00\bar{R}^4}{g(C-A)} \int_0^{2\pi} p_{\mathrm{s}} \cos^2\phi \sin\phi\,(\cos\lambda, \sin\lambda)\,\mathrm{d}\lambda, \tag{2.2a}$$

$$(\xi_1^{\mathrm{w}}, \xi_2^{\mathrm{w}}) \equiv \frac{-1.43\bar{R}^3}{g(C-A)\,\Omega} \int_0^{p_{\mathrm{s}}} \int_0^{2\pi} \cos\phi\,\{u \sin\phi\,(\cos\lambda, \sin\lambda) - v\,(\sin\lambda, -\cos\lambda)\}\,\mathrm{d}\lambda\,\mathrm{d}p \tag{2.2b}$$

and

$$(\xi_3^{\mathrm{p}}, \xi_3^{\mathrm{w}}) \equiv \left(\frac{0.70\bar{R}^4}{gC} \int_0^{2\pi} p_{\mathrm{s}} \cos^3\phi\,\mathrm{d}\lambda, \quad \frac{\bar{R}^3}{gC\Omega} \int_0^{p_{\mathrm{s}}} \int_0^{2\pi} u \cos^2\phi\,\mathrm{d}\lambda\,\mathrm{d}p \right). \tag{2.3}$$

In these expressions, (ϕ, λ) denote latitude and longitude respectively, $p_{\mathrm{s}}(\phi, \lambda, t)$ is the surface pressure and $u(\phi, \lambda, p, t)$ and $v(\phi, \lambda, p, t)$ are the eastward and northward components respectively of the wind velocity at pressure level p. In the calculations presented here, we follow BHWW who took $\bar{R} = 6.37 \times 10^6$ m for the mean radius of the solid Earth, $\Omega = 7.29 \times 10^{-5}$ rad s^{-1} for its mean rotation rate, $g = 9.81$ m s^{-2} for the mean acceleration due to gravity, $C = 7.04 \times 10^{37}$ kg m^2 for the polar moment of inertia of the solid Earth, and $(C-A)/A = 3.33 \times 10^{-3}$ where A is the corresponding equatorial moment of inertia. The coefficients 1.00, 1.43 and 0.70 incorporate the so-called 'Love number' corrections which allow for concomitant meteorologically induced tiny but dynamically significant changes in the inertia tensor of the slightly deformable solid Earth. The dimensionless pseudo-vector χ_i is related to the AAM vector H_i, with the equatorial components (χ_1, χ_2) and (H_1, H_2) scaled differently from the axial components χ_3 and H_3 (see equations (2.1)–(2.3)).

Any change in H_3 is accompanied by an equal and opposite change in the axial component of the angular momentum of the solid Earth (since the fluctuations in the azimuthal motion of the underlying liquid core of moment of inertia *ca.* $0.1C$ are

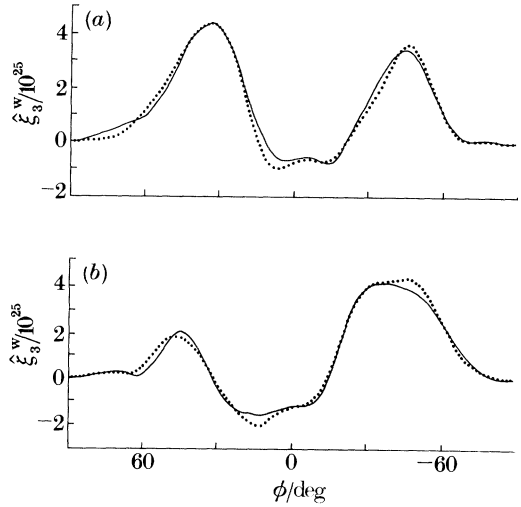

Figure 4. (*a*) Distribution with respect to ϕ (latitude) of $\hat{\xi}_3^{\mathrm{w}}$, defined as the monthly-mean value of the wind contribution to the dimensionless quantity $\xi_3^{\mathrm{w}}(\phi, t)$ (see equation (2.3)) for January 1988, and (*b*) July 1988 (cf. figure 2). The integral of ξ_3^{w} from $\phi = -\frac{1}{2}\pi$ to $\phi = \frac{1}{2}\pi$ is proportional to the wind contribution to the axial component of the angular momentum of the atmosphere. The full lines are based on ECMWF 'analyses' and the dotted lines on the ECMWF forecasts out to 10 d reported in this paper.

effectively decoupled from those of the solid Earth on the short timescales with which we are concerned here (see Hide *et al.* 1980)). In terms of the dimensionless quantities m_3 and χ_3 (see equations (1.3) and (2.1)–(2.3)), this can be expressed as

$$\dot{m}_3 + \dot{\chi}_3 = 0 \tag{2.4}$$

with solution

$$m_3(t) + \chi_3(t) = m_3(t_0) + \chi_3(t_0), \tag{2.5}$$

where $m_3(t_0)$ and $\chi_3(t_0)$ are constants of integration equal respectively to the values of m_3 and χ_3 at some initial instant $t = t_0$. The dominant contribution to fluctuations in χ_3 comes from the 'wind' term χ_3^{w}, which depends (see equations (2.1) and (2.3)) on the distribution in the meridional plane of the average with respect to longitude λ of the eastward (westerly) wind speed (see figures 2 and 4).

When applied to changes in the equatorial components of H_i, Euler's dynamical equations give

$$\mathrm{i}\sigma^{-1}\dot{\boldsymbol{m}} + \boldsymbol{m} = \boldsymbol{\chi} - \mathrm{i}\Omega^{-1}\dot{\boldsymbol{\chi}}, \tag{2.6}$$

where $\boldsymbol{\chi} \equiv \chi_1 + \mathrm{i}\chi_2$ and

$$\sigma \equiv \sigma_{\mathrm{R}} + \mathrm{i}\sigma_{\mathrm{I}} \tag{2.7}$$

is a complex frequency (see BHWW and Hide 1984). $2\pi\sigma_{\mathrm{R}}^{-1}$ is the observed chandlerian period (435 d) and σ_{I} is the inverse time constant that measures the rate at which various damping processes would attenuate the chandlerian wobble if the excitation mechanism were suddenly turned off. Estimates of $\sigma_{\mathrm{R}}/(2\pi\sigma_{\mathrm{I}})$ range from 10 to well in excess of 10^2 (see Lambeck 1980). (See equations (A 1) and (A 2) for solutions to equation (2.6).)

In the practical determination of the χ_i time series, frequent wind and pressure data are needed over the whole globe and up to the highest possible levels in the atmosphere. During the two 'special observing periods' (between 5 January and 5 March 1979 and 1 May and 30 June 1979) of the 'First GARP Global Experiment'

(FGGE) (see Appendix A), meteorologists made a special effort to obtain good data coverage to high levels, well into the stratosphere, not only in extra-tropical regions in the Northern Hemisphere but also in the Tropics and the extra-tropical Southern Hemisphere. Routine meteorological observations and data processing are better now than they were before FGGE, but observations are still less abundant in the stratosphere and the troposphere in the Tropics and Southern Hemisphere than they are in the extra-tropical regions of the Northern Hemisphere troposphere. There are concomitant uncertainties of up to about 10% in individual determinations of χ_3 that are now made routinely at various meteorological centres, and rather more than 10% in determinations of $|\boldsymbol{\chi}|$.

The irregular distribution of the meteorological data makes it impracticable to calculate H_i and χ_i time series directly from the 'raw' observations. Determinations of the series are best made from the global analyses of meteorological variables, which are generated routinely by the numerical data assimilation systems (described below) and used as initial conditions for the numerical weather prediction models. Such models or systems are designed to predict, on an objective and quantitative basis, how the atmosphere will evolve from its present state as time progresses. So the essential ingredients of a prediction model are: (*a*) the observational data required to specify the state of the atmosphere at the chosen initial instant, (*b*) mathematical equations with the requisite boundary conditions expressing the laws of dynamics and thermodynamics that govern atmospheric flow and its time evolution, and (*c*) extensive data collection systems and a very powerful computer, so that the observational data can be assimilated and the governing equations integrated very rapidly. Since their introduction in the 1950s, numerical weather prediction models have developed greatly in sophistication and performance, and a number of GNWP models are currently used operationally at meteorological centres in several countries. The GNWP models of the UKMO and ECMWF were used in the present study.

The current UKMO model, introduced in 1982, is documented by Bell & Dickinson (1987). It is used operationally to provide guidance to forecasters on timescales of 12 h to 6 d (see Mason 1986). Observational data are used to guide the model towards the observed state as it is integrated over the so-called 'assimilation period' (see Bengtsson *et al.* 1981; Lorenc 1986). The governing partial differential equations are converted into 'difference equations' defined on a latitude–longitude grid at 15 unequally spaced σ-levels (surfaces of constant values of

$$\sigma(x, y, z, t) \equiv p(x, y, z, t)/p_s(x, y, t))$$

in the vertical. On the top level $p = 0.025\ p_s$, and on the bottom level $p = 0.997\ p_s$. The model has horizontal grid lengths of 1.875° along lines of latitude and 1.5° along lines of longitude, giving a total of $15 \times 192 \times 121 = 348\,480$ grid points in all. Evaluations of the eastward and northward wind components (u, v), the vertical velocity, potential temperature, specific humidity and geopotential are held in each grid box. Thus about 1.5×10^6 data are used to specify the state of the atmosphere at a given instant $t = T$ (say).

The representation of subgrid scale processes (small-scale convection, radiative transfer, turbulent boundary-layer drag, surface orography, etc.) in GNWP models is a matter of great importance, upon which much research remains to be done. Bell & Dickinson (1987) outline the methods whereby these processes are parametrized in the UKMO GNWP model. Among the factors that render the present model suitable

PHILOSOPHICAL TRANSACTIONS OF THE ROYAL SOCIETY A MATHEMATICAL, PHYSICAL & ENGINEERING SCIENCES

for AAM determinations is the 'gravity-wave drag' method used for representing the stress exerted at all levels in the atmosphere resulting from the interaction of surface winds with subgrid scale orography (see Palmer *et al.* 1986; McFarlane 1987; Miller *et al.* 1989).

Detailed accounts of aspects of the GNWP model currently in operational use at the ECMWF can be found in papers by Simmons *et al.* (1989) on the adiabatic formulation of the model; by Tiedtke *et al.* (1988) and Miller *et al.* (1989) on parametrization schemes; and by Shaw *et al.* (1987) on the analysis scheme. Horizontal discretization of the governing partial differential equations is carried out by means of the spectral method, while in the vertical a hybrid coordinate is used, for which the upper-level model surfaces flatten over steep terrain, becoming surfaces of constant pressure in the stratosphere (Simmons & Burridge 1981). Observational data increments calculated at six-hourly intervals are interpolated on to a regular analysis grid and added to the model's 6 h forecast field. Currently, triangular truncation at horizontal spherical harmonic of order 106 is used. The model's 19 unequally spaced hybrid pressure levels range from the surface up to 10 mbar. As well as a parametrization of gravity wave drag, the ECMWF model has an enhanced orography, as described in Wallace *et al.* (1983) and Jarraud *et al.* (1988), rather than a grid-box mean orography of the type incorporated in the UKMO model.

The quality of the observational data and their distribution and of the analyses themselves are assessed continuously (see, for example, Hollingsworth 1987; Hollingsworth *et al.* 1985; Hollingsworth *et al.* 1986; Lambert 1988; Trenberth & Olsen 1988). Assessments and intercomparisons of model forecasts have also been reported in the literature (see, for example, Arpe *et al.* 1985; Arpe & Klinker 1986; Lange & Tokkola 1988; Klinker & Sardeshmukh 1988; Caplan & White 1989). Various methods have been used for evaluating and intercomparing the AAM time series calculated from the analyses of various meteorological centres (see, for example, Rosen *et al.* 1987*a*; Naito *et al.* 1987; Salstein 1987; Sakellarides 1989; Bell & Nitsas 1989). Forecasts of the axial component of AAM have been presented by Rosen *et al.* (1987*b*).

The UKMO determinations of the dimensionless AAM functions are presented in the following sections. They were obtained by direct area-weighted integration of equations (2.1)–(2.3) using the model wind fields on the 15 σ-levels. The vertical integrations were performed using the trapezoidal rule with the lower limit of the integral at the level $\sigma = 0.997$ ($p \approx 1000$ mbar) and the upper limit at $\sigma = 0.025$ ($p \approx 25$ mbar). The matter terms χ_i^{p} were evaluated using the pressure field at the bottom surface ($\sigma = 1$). The ECMWF determinations used the model fields transformed on to a gaussian grid with appropriate resolution (320 equally spaced points on each of 160 gaussian latitudes). The vertical integrals for the wind terms χ_i^{w} were performed using the rectangular rule with the practical limits of the integral corresponding to the theoretical limits, namely $p = p_{\mathrm{s}}$ and $p = 0$. Thus it was effectively assumed that winds above the $p = 10$ mbar level are independent of height. The matter terms χ_i^{p} (see equations (2.1)–(2.3)) were evaluated using the pressure on the lowest level represented within the model. Unless explicitly stated to the contrary, the ECMWF AAM values were based on 'initialized' meteorological fields, obtained from the 'analysis' fields by filtering out unbalanced features using a nonlinear normal mode initialization procedure (see Daley 1981).

3. Analyses and forecasts of changes in the axial component of AAM

The forecasts of each component of AAM (and of various contributions thereto) have been assessed by comparing forecast changes with corresponding analysis changes. Their discussion in this section and in §5 will be facilitated by using the following notation. Denote by $W(t)$ the analysis value of any quantity W, valid at time t (where t is measured in days), and by $W(t;n^*)$ the 'n-day forecast' value of W valid at time t (i.e., the forecast made n-days before time t). The quantity

$$\Delta W(t;n) \equiv W(t)-W(t-n) \tag{3.1}$$

is the 'n-day analysis change' in W at time t; correspondingly

$$\Delta W(t;n^*) \equiv W(t;n^*)-W(t-n) \tag{3.2}$$

is the 'n-day forecast change' in W at time t.

For a set $\{X_q\}$, $q = 1, \ldots, N$, of N forecast or analysis changes, $\bar{X}$ will denote the arithmetic mean of X_q and X'_q the deviation of X_q from the mean:

$$\bar{X} \equiv N^{-1} \sum_{q=1}^{N} X_q, \quad X'_q \equiv X_q-\bar{X}. \tag{3.3}$$

For a second set, $\{Y_q\}$, of N forecast or analysis changes valid at the same times as the set $\{X_q\}$, S will denote the root mean square (r.m.s.) of the difference between the X'_q and Y'_q, whence

$$S^2 \equiv (N-1)^{-1} \sum_{q=1}^{N} (X'_q-Y'_q)^2; \tag{3.4}$$

R^2 is the square of the correlation coefficient

$$R^2 \equiv \left(\sum_{q=1}^{N} X'_q Y'_q \right)^2 \Big/ \left(\sum_{q=1}^{N} (X'_q)^2 \sum_{q=1}^{N} (Y'_q)^2 \right); \tag{3.5}$$

and G is the regression slope defined as follows:

$G \equiv$ slope of the straight line through the points with coordinates (X_q, Y_q), $q = 1, \ldots, N$, for which the sum of the square perpendicular deviations of all points is a minimum. (3.6)

If $\{Y_q\}$ is a set of forecast changes all with the same lead-time, n, and $\{X_q\}$ is the corresponding set of analysis changes, then

$$B \equiv \bar{Y}-\bar{X} \tag{3.7}$$

is the 'mean forecast bias'. Finally, if the data $\{X_q\}$ are valid on consecutive days, the (sample time-lagged) autocorrelation function $A(K)$ is

$$A(K) \equiv \sum_{q=1}^{N-K} X'_q X'_{q+K} \Big/ \sum_{q=1}^{N} (X'_q)^2. \tag{3.8}$$

These quantities have been calculated for various seasons; each winter (WI) season covers 3 December–2 March, spring (SP) 3 March–2 June, summer (SU) 3 June–

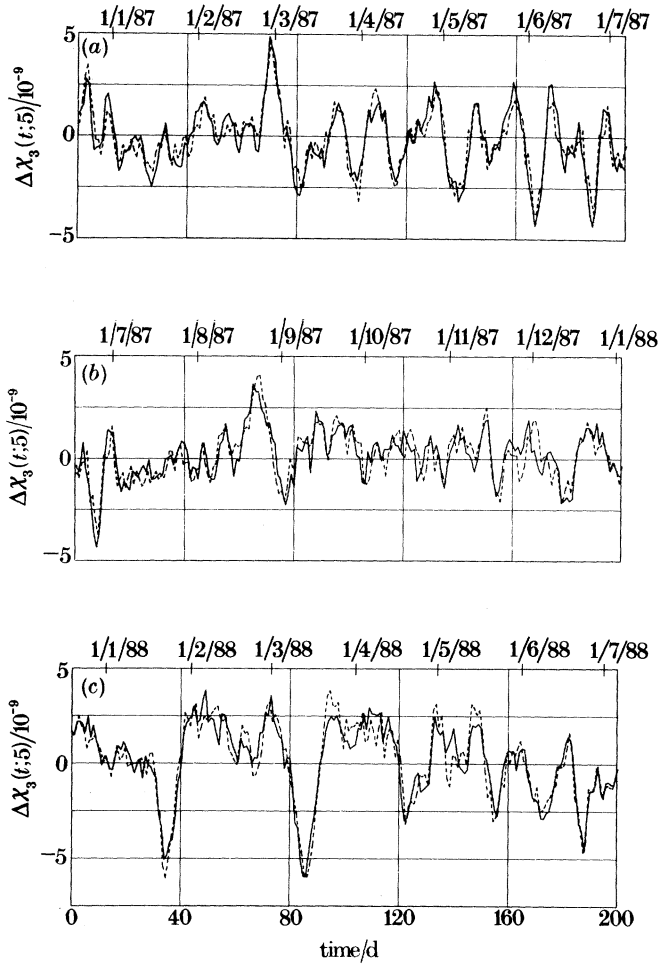

Figure 5. Fluctuations in $\Delta\chi_3(t;5)$ during (*a*) January 1987 to July 1987, (*b*) July 1987 to January 1988, and (*c*) January 1988 to July 1988. $\Delta\chi_3(t;5)$ is the analysis change in 5 d of $\chi_3(t)$ (see equation (3.1)). The full lines are based on UKMO analyses for 00Z and the dashed lines on ECMWF analyses for 12Z. The bottom axes are: in (*a*) day after 1 January 1975 (day zero) minus 4370; in (*b*), day after 1 January 1975 minus 4550; in (*c*), day after 1 January 1975 minus 4735.

2 September, and autumn (AU) 3 September–2 December. For 5 d changes (see equations (3.1) and (3.2)) these seasons coincide closely with standard season definitions.

As a preliminary to comparing forecasts of the axial component, we display in figure 5 the time series of $\Delta\chi_3(t;5)$, 5 d analysis changes in χ_3, according to the UKMO and ECMWF operational GNWP models for (*a*) January–July 1987, (*b*) July 1987–January 1988 and (*c*) January–July 1988. The magnitude of the largest fluctuations, 5×10^{-9}, exceeds half the peak to trough amplitude of a typical annual cycle in χ_3. The agreement between the two time series is clearly very good. Table 1 gives R^2 and S (see equations (3.5) and (3.4)) for these time series for each of the eight seasons between WI86–7 and AU88. R^2 is close to 0.9 except during WI86–7 ($R^2 = 0.78$) and AU87 ($R^2 = 0.61$). S shows proportionately smaller variations between seasons than does R^2, averaging 0.55×10^{-9}.

Table 1. *Statistical assessment of 5 d analysis changes in* χ_3, $\Delta\chi_3(t_q;5)$, *made by comparison of changes according to UKMO,* X_q, *with those from ECMWF,* Y_q, *for each season from winter 1986–7 to autumn 1988.* (R^2 *is defined by equation (3.5) and* S *by (3.4))*

season	R^2	$10^9 S$
WI86–7	0.78	0.65
SP87	0.89	0.50
SU87	0.87	0.59
AU87	0.61	0.61
WI87–8	0.90	0.55
SP88	0.92	0.61
SU88	0.89	0.52
AU88	0.88	0.47

The significance of the difference between the values of R^2 in AU87 and AU88 can be formally assessed using Fisher's 'Z distribution' (Kendall & Stuart 1977, vol. I, §16.33), namely

$$Z \equiv \operatorname{arctanh} R. \tag{3.9}$$

This function has a near-normal distribution with

$$\operatorname{var} Z \approx (N' - 3)^{-1}, \tag{3.10}$$

where N' is the number of independent data in the sample. The interdependence of data on successive days has been assessed by calculating $A(K)$, the autocorrelation function, for three 200 d intervals of the time series of $\Delta\chi_3(t;5)$ from UKMO and ECMWF analyses. The three intervals covered December 1986–June 1987, June–December 1987, and December 1987–June 1988. For the first of these intervals, $A(K)$ first changes sign when $K = 4$ (i.e., at a time lag of 4 d). The magnitude of $A(K)$ is smaller than 0.3 for $K \geqslant 4$ in all three intervals. It is thus reasonable to set $N' = 0.2N \approx 18$ in equation (3.10). The difference between Z in AU87 and AU88, which is 0.67, can hence be compared with the variance of the difference, namely 0.13. The hypothesis that the difference between Z in AU87 and in AU88 has zero mean may then be rejected with a confidence level of 90% but not 95%. Many similar tests could have been performed on pairs of data selected from table 1, so it is likely that at least one pair (e.g., the one chosen) will appear to have significantly different members (at the 5% level). So the difference between the values of R^2 in the two autumns probably indicates neither an exceptional season nor a change in data quality.

The generally good agreement in figure 5 is obtained despite the fact that χ_3 receives large contributions from upper levels in the tropics and Southern Hemisphere, where data coverage is significantly sparser than for N.W. Europe and N. America and for which uncertainties in the analyses are correspondingly large (Bengtsson *et al.* 1982; Hollingsworth *et al.* 1986, figure 3; Trenberth & Olsen 1988; Lambert 1988). The agreement indicates that the $\Delta\chi_3(t;5)$ time series provides suitable reference data for the assessment of 5 d forecasts. This is evidently not so for 1 d analysis changes, $\Delta\chi_3(t;1)$, for the correlation between the respective time series of $\Delta\chi_3(t;1)$ from UKMO and ECMWF ranges from $R^2 = 0.45$ in SU87 to $R^2 = 0.71$ in SP88; the corresponding seasonal values of S average 0.38×10^{-9}. The possibility that coherent errors in the UKMO and ECMWF analysis changes could be detected by comparisons with geodetic data on fluctuations in Λ (see equations (1.6a) and (2.5)) is discussed in §4.

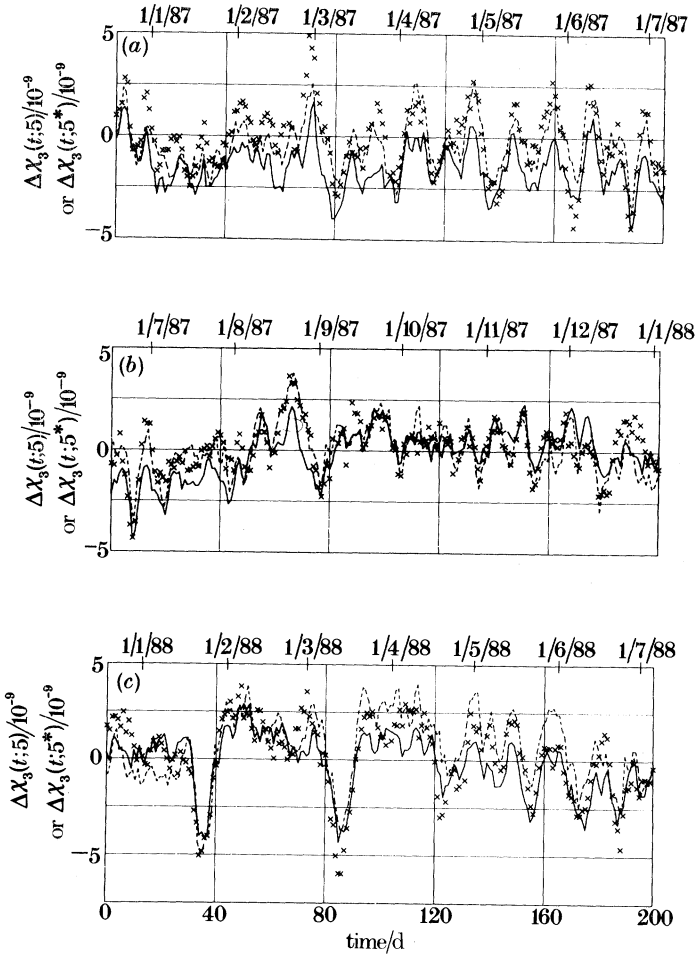

Figure 6. Time series of $\Delta\chi_3(t;5)$ and $\Delta\chi_3(t;5^*)$ for (*a*) January 1987 to July 1987, (*b*) July 1987 to January 1988, and (*c*) January 1988 to July 1988 (cf. figure 5). $\Delta\chi_3(t;5^*)$ is the 5 d forecast change in $\chi_3(t)$ defined by equation (3.2) and $\Delta\chi_3(t;5)$ the analyses change in $\chi_3(t)$ defined by equation (3.1). The crosses give $\Delta\chi_3(t;5)$ calculated using UKMO data, the continuous curve is $\Delta\chi_3(t;5^*)$ based on UKMO data, and the dashed line is $\Delta\chi_3(t;5^*)$ based on ECMWF data. The bottom axes are as for figure 5.

Time series of $\Delta\chi_3(t;5^*)$, namely 5 d forecast changes in χ_3, according to UKMO and ECMWF for the same periods as for figure 5 are displayed in figure 6. They exhibit three features of note. First, forecast and analysis changes are well correlated. Secondly, it is evident that the UKMO forecast changes have a smaller mean value during the first half of 1987 than do the analysis changes, with the mean forecast-change bias during this period corresponding to a steady loss of relative angular momentum in the UKMO model at about 0.8 % per day. Finally, the amplitudes of the UKMO and ECMWF forecast changes tend to be systematically smaller than those exhibited by analysis changes. These three features are evident in the scatter plot of figure 7 for SP87 in which the UKMO $\Delta\chi_3(t;5^*)$ is given on the ordinate against the UKMO $\Delta\chi_3(t;5)$ on the abscissa. The continuous line passing through the points is the straight line with slope G (see equation (3.6)).

PHILOSOPHICAL TRANSACTIONS OF THE ROYAL SOCIETY A MATHEMATICAL, PHYSICAL & ENGINEERING SCIENCES

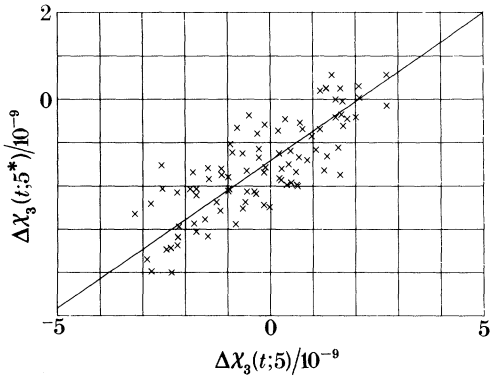

Figure 7. Scatter plot presenting 5 d forecast and 5 d analysis changes in $\chi_3(t)$ for the spring of 1987 calculated using UKMO data (see figure 6*a*). $\Delta\chi_3(t;5)$ is plotted on the abscissa and $\Delta\chi_3(t;5^*)$ on the ordinate. The straight line through the data is that for which the sum of the square perpendicular distances to all the points is a minimum (see equation (3.6) and table 2).

Table 2. *Statistical assessment of 5* d *forecast changes in* χ_3, $\Delta\chi_3(t_q;5^*) \equiv Y_q$, *made by comparison with 5* d *analysis changes in* χ_3, $\Delta\chi_3(t_q;5) \equiv X_q$, *for each season from winter 1986–7 to autumn 1988.* (S, R^2, G *and* B *are defined by equations* (3.4)–(3.7))

	R^2		G	
season	UKMO	ECMWF	UKMO	ECMWF
WI86–7	0.51	0.71	0.70	0.80
SP87	0.63	0.74	0.68	0.89
SU87	0.68	0.75	0.77	0.95
AU87	0.51	0.53	0.78	1.00
WI87–8	0.59	0.68	0.74	0.97
SP88	0.77	0.85	0.66	0.79
SU88	0.71	0.68	0.70	0.86
AU88	0.62	0.72	0.84	0.95

	10^9B		10^9S	
season	UKMO	ECMWF	UKMO	ECMWF
WI86–7	−1.35	−0.63	0.97	0.68
SP87	−1.34	−0.05	0.89	0.72
SU87	−0.91	0.18	0.93	0.78
AU87	0.08	−0.01	0.65	0.72
WI87–8	0.01	−0.30	1.06	0.99
SP88	−0.34	1.03	0.99	0.84
SU88	−0.59	0.44	0.80	0.86
AU88	−0.60	0.22	0.72	0.73

Further information on these features is contained in table 2 which gives statistical properties of the $\Delta\chi_3(t;5^*)$ for each season from WI86–7 to AU88. According to table 2, R^2 for these forecasts fluctuates substantially from season to season; for example, ECMWF has $R^2 = 0.53$ in AU87 and $R^2 = 0.85$ in SP88. The average UKMO correlation is around 0.63 and that of ECMWF around 0.70. It is noteworthy that the lowest correlation for ECMWF occurred in AU87, the season when the correlation between UKMO and ECMWF analysis changes was also at its lowest (see table 1).

PHILOSOPHICAL TRANSACTIONS OF THE ROYAL SOCIETY A MATHEMATICAL, PHYSICAL & ENGINEERING SCIENCES

Table 3. *The correlation (R^2) between analysis and forecast changes and the mean forecast bias (B) of 5 and 10* d *forecasts of χ_3 made by ECMWF for each season from spring 1986 to autumn 1988*

	R^2		10^9B	
season	EC5	EC10	EC5	EC10
SP86	0.83	0.75	0.40	0.03
SU86	0.66	0.49	0.40	0.03
AU86	0.73	0.62	−0.29	−1.28
WI86–7	0.71	0.37	−0.63	−1.60
SP87	0.74	0.29	−0.05	−0.95
SU87	0.75	0.77	0.18	−0.50
AU87	0.53	0.39	−0.01	−0.69
WI87–8	0.68	0.58	−0.30	−0.64
SP88	0.85	0.80	1.03	0.60
SU88	0.68	0.67	0.44	0.86
AU88	0.72	0.50	0.22	−0.20

UKMO forecasts also had their joint lowest correlation with UKMO analyses during this period. The regression slope for the UKMO forecasts fluctuates around 0.7 and the ECMWF slope averages about 0.8; both forecast models, particularly that of UKMO, have a systematic tendency to predict smaller amplitude changes than actually occur. It is interesting that high values of R^2 and values of G close to 1.0 do not show any positive correlation. For example, ECMWF in SP88 has a high value of R^2 (0.85) and low value of G (0.79) and in AU87 a lower value of R^2 (0.53) and higher value of G (1.00).

As is evident from table 2, the seasonal mean forecast biases (B) of both models are also subject to substantial variations. The fluctuations in the UKMO data occurred despite the fact that there were no major modifications to the assimilation system, forecast model or data sources over the two-year period covered by table 2. The formal significance of the apparent difference between WI86–7 and WI87–8 has been assessed by testing the hypothesis that the difference between the biases has zero mean. Using the r.m.s. difference values of table 2 and $N' = \frac{1}{5}N$ (as above) in a Student's t-test, it is found that the hypothesis can be rejected with 99.9% confidence.

The source of the variation for the UKMO model is elucidated by figure 8, which presents meridional cross sections of analysis and forecast bias values of $\bar{u}(\phi, p)$, the time-mean zonally averaged westerly wind (in m s^{-1}) for December 1986–February 1987 and December 1987–February 1988. The main differences between the bias cross sections are the reduction of the negative bias present in the earlier period at upper levels in the tropics (i.e., between 20° S and 20° N and above 300 mbar) and the development of positive biases in the later period on the equatorial sides of the subtropical jets at upper levels (i.e., around 250 mbar at 20° S and also 20° N). The decrease in the tropical easterlies at 100 mbar from the earlier to the later period, which is associated with the 'quasi-biennial oscillation' of the upper level zonal winds in the tropics, is in the same sense as the change in the forecast bias. Maps (not shown) of the 5 d forecast bias in the zonal winds at 100 mbar and 250 mbar reveal that in the earlier period the excessive easterlies cover most of the equatorial belt between 20° S and 20° N and have local maximum seasonal mean errors exceeding 10 m s^{-1}.

PHILOSOPHICAL TRANSACTIONS OF THE ROYAL SOCIETY A MATHEMATICAL, PHYSICAL & ENGINEERING SCIENCES

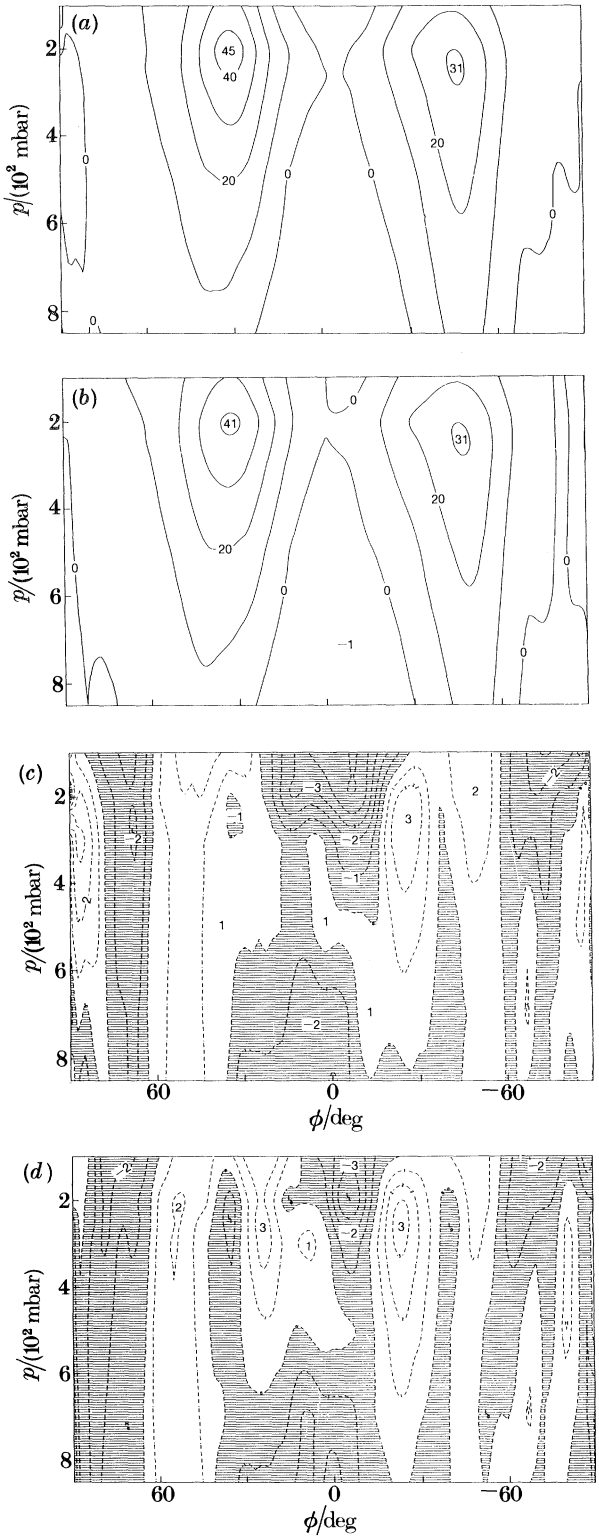

Figure 8. For description see opposite.

PHILOSOPHICAL TRANSACTIONS OF THE ROYAL SOCIETY A MATHEMATICAL, PHYSICAL & ENGINEERING SCIENCES

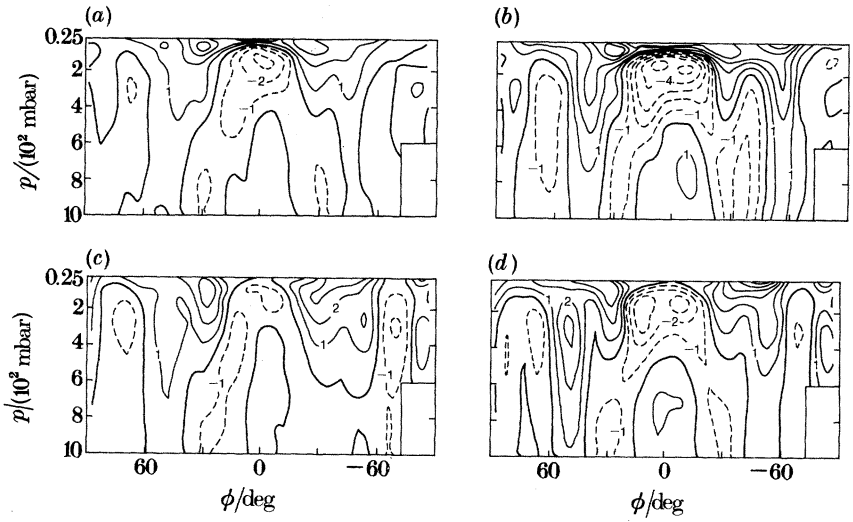

Figure 9. Meridional cross sections of forecast error fields of the time-mean zonally averaged westerly wind, $\bar{u}(\phi, p)$ (in m s^{-1}), produced by the ECMWF GNWP model for March to May 1987, (*a*) 5 d forecasts, (*b*) 10 d forecasts; and March to May 1988, (*c*) 5 d forecasts, (*d*) 10 d forecasts. (Figure provided by Dr K. Arpe.)

Table 3, giving seasonal values of B and R^2 for the ECMWF forecasts of $\Delta\chi_3(t;5)$ and $\Delta\chi_3(t;10)$ between SP86 and AU88, shows that there were similar jumps in B for these ECMWF forecasts between WI86–7 and SP88. Some information on the geographical location of the origin of these jumps is presented in figure 9, which gives meridional cross sections of the 5 d and 10 d mean forecast biases for (*a*) March–May 1987 and (*b*) March–May 1988. A reduction in the easterly bias at levels above 300 mbar in the Tropics makes a major contribution to these bias changes, particularly that in the ten-day forecast. Tibaldi *et al.* (1987), Milton & Dickinson (1988) and Tibaldi *et al.* (1990) have found the mean easterly forecast bias to be even larger in the high level tropical easterlies in longer integrations of the ECMWF and UKMO models. A strengthening of the positive bias in the mid-latitude westerlies is also an important factor in the 5 d bias change from the earlier to the later period. Though the changes in these bias cross sections are somewhat similar to those of figure 8, a substantial alteration to the forecast model, introduced on 5 January 1988, restricting the main vertical diffusion of momentum to the surface boundary layer in the ECMWF forecast model (Miller 1988), was probably largely responsible for the changes, since they occurred abruptly between winter 1987 and spring 1988.

As well as the abrupt change in B between winter 1987 and spring 1988, just discussed, table 3 shows that there was an abrupt change between summer 1986 and autumn 1986. The latter was probably the result of introducing into the ECMWF model on 15 July 1986 a parametrization of the momentum transport by gravity waves generated by orographic variations with smaller scales than the separation of

Figure 8. Meridional cross sections of the average analysis fields ((*a*) and (*b*)), and the average 5 d forecast error fields of $\bar{u}(\phi, p)$ ((*c*) and (*d*)), the time-mean zonally-averaged westerly wind (in m s^{-1}), produced by the UKMO GNWP model for ((*a*) and (*c*)) December 1986 to February 1987, and ((*b*) and (*d*)) December 1987 to February 1988 (*cf.* figure 2). (Figure provided by Miss W. L. Adams.)

PHILOSOPHICAL TRANSACTIONS OF THE ROYAL SOCIETY A MATHEMATICAL, PHYSICAL & ENGINEERING SCIENCES

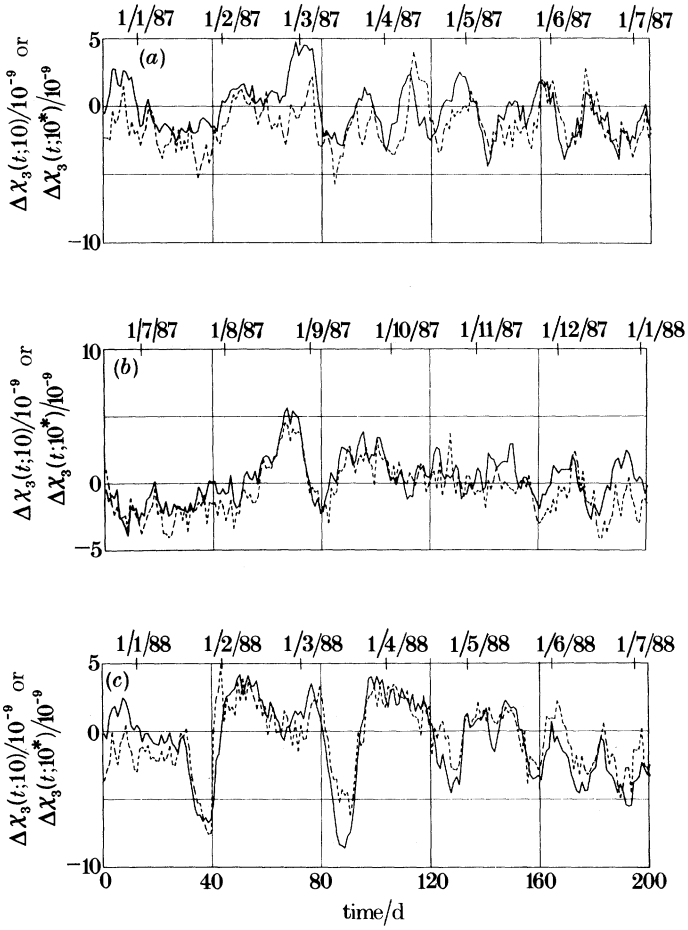

Figure 10. Time series of 10 d changes in 12Z analyses of $\chi_3(t)$, namely $\Delta\chi_3(t;10)$ (continuous curve), and the corresponding forecast change $\Delta\chi_3(t;10^*)$ (dashed curve) for: (*a*) January to July 1987, (*b*) July 1987 to January 1988, and (*c*) January 1988 to July 1988. The bottom axes are as for figure 5*a–c*.

grid points of the forecast model (Miller *et al.* 1989). The immediate impact on B of restricting the diffusion to the boundary layer, for both 5 and 10 d forecast changes of χ_3, appears to be at least comparable in magnitude with that of the gravity wave parametrization, although uncertainty in the natural variation in B makes accurate assessment impossible at this stage. Gravity wave parametrization had a greater impact on the UKMO model than on the ECMWF model, which already included an envelope orography. Because the gravity wave parametrization was introduced into the UKMO model before operational calculations of AAM forecasts began, we are unable here to give a quantitative assessment of its impact.

Table 3 also shows that seasonal values of R^2 for 10 d forecasts of $\Delta\chi_3$ by ECMWF are more variable than those of 5 d forecasts. The maximum value attained for 10 d forecasts was 0.80 (SP88) and the minimum 0.29 (SP87). Figure 10 presents the time series of $\Delta\chi_3(t;10^*)$ and $\Delta\chi_3(t;10)$ (cf. figure 6 for $\Delta\chi_3(t;5^*)$).

More detailed information on the dependence of the forecast performance on the length of the forecast during (*a*) SP88 and (*b*) AU88 is given in table 4. Particularly striking are the comparatively small correlation coefficients R^2 of the 1 d forecasts.

PHILOSOPHICAL TRANSACTIONS OF THE ROYAL SOCIETY A MATHEMATICAL, PHYSICAL & ENGINEERING SCIENCES

Table 4. *Statistical assessment of the dependence on n of changes of χ_3 as forecast for n* d *ahead by UKMO and ECMWF for spring 1988 and autumn 1988 (cf. table 2)*

	spring 1988, UKMO					spring 1988, ECMWF			
n	R^2	G	10^9B	10^9S	n	R^2	G	10^9B	10^9S
1	0.56	0.58	−0.23	0.40	1	0.54	0.63	0.00	0.47
2	0.71	0.68	−0.31	0.55	2	0.73	0.80	0.26	0.56
3	0.75	0.69	−0.38	0.69	3	0.83	0.84	0.59	0.59
4	0.78	0.68	−0.40	0.82	4	0.81	0.83	0.86	0.72
5	0.77	0.67	−0.37	0.99	5	0.85	0.79	1.03	0.84
6	0.75	0.65	−0.35	1.17	10	0.80	0.70	0.60	1.51

	autumn 1988, UKMO					autumn 1988, ECMWF			
n	R^2	G	10^9B	10^9S	n	R^2	G	10^9B	10^9S
1	0.49	0.52	−0.34	0.40	1	0.59	0.79	−0.19	0.34
2	0.67	0.68	−0.49	0.48	2	0.72	0.85	−0.17	0.45
3	0.68	0.74	−0.60	0.55	3	0.71	0.94	−0.02	0.59
4	0.65	0.79	−0.65	0.64	4	0.78	0.92	0.08	0.58
5	0.62	0.84	−0.60	0.72	5	0.72	0.95	0.22	0.73
6	0.59	0.80	−0.57	0.83	10	0.50	1.20	−0.20	1.44

The corresponding correlation coefficients for UKMO and ECMWF one-day analysis changes are also low; $R^2 = 0.71$ (SP88) and $R^2 = 0.69$ (AU88). The application of a low-pass filter to the data, which removes fluctuations with periods of 7 d or less and retains those of 20 d or more, increases the correlation between forecast and analysis changes and decreases the variation from season to season. The filter used was devised by Vondrák (1977) and applied with smoothing parameter $\epsilon = 10^{-2}$ (see his fig. 1). Hence, much of the 'skill' of the forecasts can be attributed to the successful prediction of variations with periods greater than about 10 d. One possible interpretation of the slow decay of the correlation coefficient R^2 (see table 4) with forecast period n is that the observed AAM changes are largely caused by those surface stresses that involve the largest horizontal scales of motion present in the atmosphere, with other scales playing a comparatively minor role (see, for example, fig. 7 of Arpe *et al.* 1985). This finding will have to be followed up by appropriate diagnostic studies of topographic and other surface stresses.

Over periods of months and years the fluctuations in χ_3 are dominated by changes in χ_3^{w}. However, on timescales as short as a few days, fluctuations in χ_3^{p} assume greater importance, being about as large as one third of those in χ_3^{w} in magnitude. Table 5 presents a similar analysis for $\Delta\chi_3^{\mathrm{p}}$ forecasts to that of table 2 for $\Delta\chi_3$ forecasts. Comparison of the two tables shows that the correlation coefficients for the forecasts $\Delta\chi_3^{\mathrm{p}}(t;5^*)$ are comparable with those for $\Delta\chi_3(t;5)$ and that the regression slopes, G, for the ECMWF forecasts $\Delta\chi_3^{\mathrm{p}}(t;5^*)$ are as good as, and for the UKMO forecasts $\Delta\chi_3^{\mathrm{p}}(t;5^*)$ better than, those of $\Delta\chi_3(t;5)$. The mean forecast error of $\Delta\chi_3^{\mathrm{p}}$ of the UKMO model is fairly steady and equivalent to that which would arise from a steady globally uniform loss of about 0.5 mbar in surface pressure over the course of the 5 d forecast period. However, the model is known to conserve mass globally more accurately than this (C. A. Wilson, personal communication), so the angular momentum loss evidently implies a tendency for the model to redistribute mass away from the equator, thereby reducing the moment of inertia of the atmosphere about the polar axis.

PHILOSOPHICAL TRANSACTIONS OF THE ROYAL SOCIETY A MATHEMATICAL, PHYSICAL & ENGINEERING SCIENCES

Table 5. *Assessment as in table 2 of 5 d forecast changes in* χ_3^p *made by UKMO and ECMWF*

	R^2		G	
season	UKMO	ECMWF	UKMO	ECMWF
WI86–7	0.54	0.69	0.85	0.93
SP87	0.59	0.66	0.86	0.90
SU87	0.63	0.73	0.91	0.82
AU87	0.71	0.68	0.85	0.90
WI87–8	0.71	0.70	0.91	0.98
SP88	0.77	0.86	0.75	0.94
SU88	0.56	0.70	0.71	1.08
AU88	0.65	0.65	0.83	0.94

	10^9B		10^9S	
season	UKMO	ECMWF	UKMO	ECMWF
WI86–7	−0.33	−0.26	0.42	0.34
SP87	−0.41	−0.23	0.43	0.36
SU87	−0.36	−0.04	0.40	0.35
AU87	−0.34	−0.01	0.33	0.34
WI87–8	−0.26	−0.06	0.33	0.31
SP88	−0.32	−0.12	0.38	0.28
SU88	−0.31	−0.13	0.37	0.29
AU88	−0.21	0.10	0.36	0.35

The performance of the 5 d forecast changes of the contributions to the wind terms of the axial AAM from the Northern Hemisphere (NH) and Southern Hemisphere (SH) are summarized in table 6. Seasonal variations in R^2 and G are proportionately larger than those exhibited by forecasts of $\Delta\chi_3$ (see table 2). A notable result is the distinct tendency for both UKMO and ECMWF forecasts of the contribution to χ_3 from the NH to have smaller values of R^2 and larger values of G in the winter seasons investigated than the summer seasons. Though less distinct, corresponding behaviour is apparent in the SH forecasts. Both models, particularly the ECMWF model, tend to have negative NH forecast biases and positive SH biases. The UKMO's NH bias reaches a minimum value during spring or summer in each of the years presented. Inspection of longer time series will of course be needed to establish whether the hemispheric biases have genuine seasonal dependences.

4. Comparison of Earth rotation and axial AAM measurements

The diurnal rotation of the Earth may be used to define a system of time. For example, the angle γ (in radians) between an inertial frame and the Greenwich meridian measured about the conventional north terrestrial pole (CTP) defines the time UT0 (in hours),

$$\mathrm{UT0} \equiv 24\gamma/2\pi \quad \text{(hours)}. \tag{4.1}$$

UT0 is an irregular time system, according to atomic clocks, partly because the CTP wobbles irregularly. A more satisfactory system, UT1, is based on the rotation angle about the celestial ephemeris pole (CEP). The CEP, which is the daily mean value of the direction of the angular momentum vector of the solid Earth, moves more slowly

Table 6. *Seasonal values of R^2, G and B for 5 d forecast changes in $\chi_3^w(NH)$ and $\chi_3^w(SH)$ made by UKMO and ECMWF*

	χ_3^w(NH)		χ_3^w(SH)	
season	UKMO	ECMWF	UKMO	ECMWF
	values of R^2			
WI86–7	0.41	0.60	0.73	0.81
SP87	0.68	0.64	0.62	0.73
SU87	0.80	0.82	0.36	0.52
AU87	0.47	0.59	0.45	0.48
WI87–8	0.61	0.62	0.56	0.71
SP88	0.75	0.76	0.66	0.84
SU88	0.83	0.82	0.65	0.66
AU88	0.68	0.68	0.69	0.82
	values of G			
WI86–7	1.25	1.16	0.66	0.76
SP87	0.59	0.81	0.70	0.68
SU87	0.72	0.86	1.14	1.23
AU87	0.92	0.83	0.73	0.86
WI87–8	0.94	0.96	0.59	0.97
SP88	0.70	0.89	0.59	0.73
SU88	0.73	0.68	0.77	0.89
AU88	0.99	1.16	0.87	0.89
	values of 10^9B			
WI86–7	−0.69	−0.63	−0.33	0.26
SP87	−0.89	0.04	−0.05	0.14
SU87	−0.84	−0.11	0.29	0.32
AU87	0.31	−0.22	0.12	0.23
WI87–8	0.19	−0.37	0.08	0.13
SP88	−0.45	0.33	0.42	0.82
SU88	−0.83	−0.13	0.55	0.69
AU88	−0.34	−0.10	−0.05	0.22

than the CTP. The time origins of both UT0 and UT1 are chosen so that on average the systems UT0 and UT1 agree as closely as possible with Greenwich Mean Time (GMT).

The length of day (LOD) (i.e., the time taken for the Earth to execute one complete rotation) is precisely 24 h by definition in the UT1 system. Fluctuations in the LOD are measured by comparing UT1 with coordinated universal time (UTC), a time system based on atomic clocks. Over a period starting at time t_1 and ending at t_2, the mean deviation of the LOD from its standard value, according to UTC, multiplied by the length of the period in days, is given by

$$(\mathrm{UTC}(t_2)-\mathrm{UT1}(t_2))-(\mathrm{UTC}(t_1)-\mathrm{UT1}(t_1)). \tag{4.2}$$

This mean value is the integral over the same time period of the difference between the instantaneous LOD, $\Lambda(t)$, and the standard LOD, Λ_0 (see equation (1.6a)). So

$$\int_{t_1}^{t_2}(\Lambda(\tau)-\Lambda_0)\,\mathrm{d}\tau = [\mathrm{UTC}\,(\tau)-\mathrm{UT1}\,(\tau)]_{t_1}^{t_2} \tag{4.3}$$

if $\mathrm{d}\tau$ is measured in days. (For further details see, for example, Moritz & Mueller 1987.)

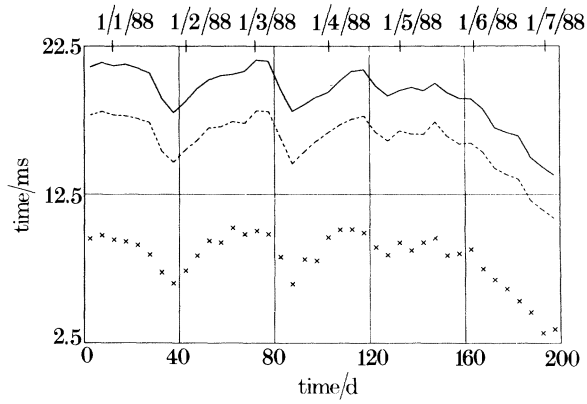

Figure 11. Illustrating changes in Universal Time over 5 d intervals from January 1988 to July 1988. Bottom graph: time series based on data from IERS (DUT1); middle and top graphs: time series based on data from angular momentum analyses (DUTA plus a constant) (ECMWF, middle graph; UKMO, top graph). (See equations (4.6) and (4.7).) The bottom axis is day after 1 January 1975 minus 4736.

As discussed in Appendix A, over periods shorter than about one year, solid Earth tides and angular momentum transfer between the atmosphere and the solid Earth are largely responsible for fluctuations in $\Lambda(t)$. From equations (1.6a) and (2.5), when effects due to solid Earth tides have been subtracted from Λ and UT1 we have

$$\Lambda(\tau)-\Lambda_0 \approx -\Lambda_0 m_3(\tau) \approx \Lambda_0(\chi_3(\tau)-\chi_3(t_0)-m_3(t_0)). \tag{4.4}$$

Hence,

$$\Lambda_0 \int_{t_1}^{t_2} (\chi_3(\tau)-\chi_3(t_0)-m_3(t_0))\,\mathrm{d}\tau = [\mathrm{UTC}\,(\tau)-\mathrm{UT1}\,(\tau)]_{t_1}^{t_2}. \tag{4.5}$$

One of the most homogeneous and accurate series of measurements of UT1 − UTC is the International Earth Rotation Service (IERS) series of values at five-day intervals. This series is based chiefly (see Appendix 3 of B.I.H. 1989) on a combination of the very long baseline interferometry (VLBI) measurements from Goddard Space Flight Centre (GSFC) and the National Geodetic Survey (NGS) in the U.S.A., and the satellite laser ranging (SLR) measurements from the Center for Space Research, University of Texas (CSR). The r.m.s. error of most of the elements in the series is quoted to be between 0.05 and 0.1 ms. We have subtracted the variations in UT1 − UTC due to solid Earth tides of all periods using the model of Yoder *et al.* (1981). For brevity we write

$$\mathrm{DUT1}(t) \equiv [\mathrm{UTC}\,(\tau)-\mathrm{UT1}\,(\tau)]_{t-2.5}^{t+2.5} \tag{4.6}$$

and

$$\mathrm{DUTA}(t) = \Lambda_0 \int_{t-2.5}^{t+2.5} \chi_3\,(\tau)\,\mathrm{d}\tau. \tag{4.7}$$

From equations (4.5)–(4.7),

$$\mathrm{DUT1}(t) = \mathrm{DUTA}(t) - \Lambda_0(m_3(t_0)+\chi_3(t_0)). \tag{4.8}$$

The IERS measurements of DUT1 for the first half of 1988 are shown by crosses on figure 11. The crosses are plotted at five-day intervals in accordance with equation (4.6) and the interval between UT1 measurements. Fluctuations in DUTA(t) calculated, using the trapezoidal rule, from UKMO 00Z analyses (full line) and

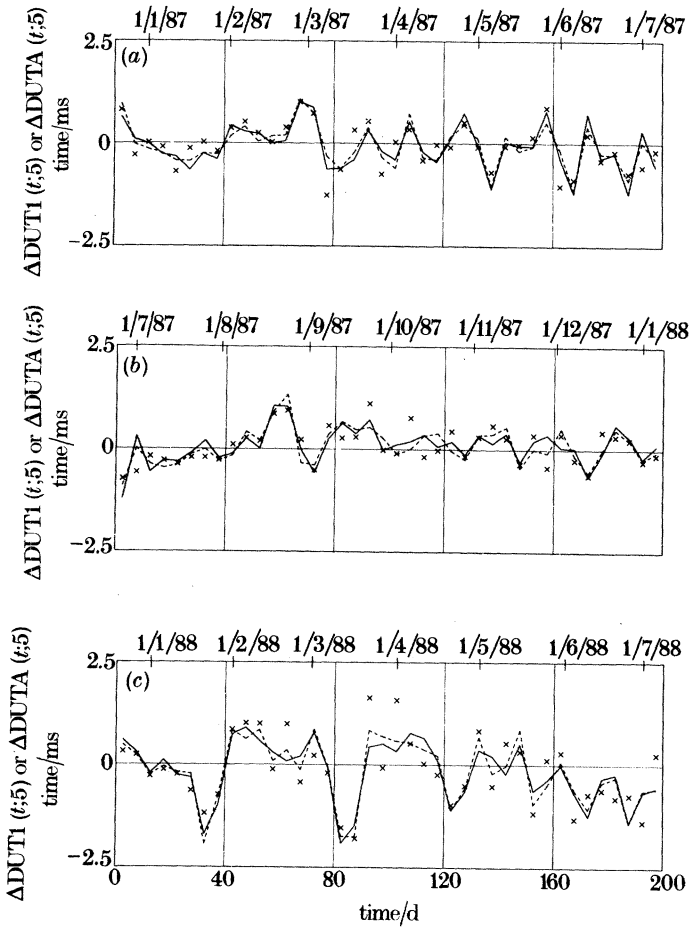

Figure 12. Time series of 5 d analysis changes in DUT1 and DUTA, namely $\Delta\mathrm{DUT1}(t;5)$ and $\Delta\mathrm{DUTA}(t;5)$ respectively (see equation (4.9)) for the intervals (*a*) January 1987 to July 1987, (*b*) July 1987 to January 1988, and (*c*) January 1988 to July 1988. Solid line, UKMO data; dashed line, ECMWF data; crosses, IERS data. The bottom axes are: in (*a*), day after 1 January 1975 (day zero) minus 4371; in (*b*), day after 1 January 1975 minus 4556; in (*c*) day after 1 January 1975 minus 4736.

ECMWF 12Z analyses (dashed line) for the same times as the values of DUT1(t) are displayed for comparison (see equation (4.8)). The offset between the values of DUTA and DUT1 has, of course, no physical significance. The offset between the UKMO and ECMWF data is due to the slight difference between the total effective atmospheric masses used in the respective models, which is associated with the different methods used for representing surface orography (see §2).

To focus on the accuracy of the measurements of the changes in the AAM occurring over 5 d periods, the '5 d analysis changes' of DUT1 and DUTA, namely

$$\Delta\mathrm{DUT1}(t;5) \equiv \mathrm{DUT1}(t) - \mathrm{DUT1}(t-5) \tag{4.9a}$$

and

$$\Delta\mathrm{DUTA}(t;5) \equiv \mathrm{DUTA}(t) - \mathrm{DUTA}\,(t-5), \tag{4.9b}$$

are displayed in figure 12. The standard error of the ΔDUT1 measurements, assuming that consecutive UT1 measurements are uncorrelated, is 2.45 ($= 6^{\frac{1}{2}}$) times that of a single UT1 measurement; i.e., between 0.12 and 0.25 ms. The level of

agreement shown in figure 12 is generally quite high, but during the pronounced rapid fluctuations that occurred in early March 1987, early June 1987 and mid to late March 1988, both the UKMO and ECMWF analyses lie well outside the two standard error bar (0.5 ms) of the $\Delta\mathrm{DUT1}(t)$ measurements. So it appears that in these instances both the UKMO and the ECMWF analysis systems underestimated the amplitudes of these rapid AAM fluctuations.

Table 7 displays seasonal values of the r.m.s. differences S and correlations R^2 between these 5 d analysis changes. The correlations between the meteorologically derived series are higher than those between the IERS series and either meteorological series. The latter are usually greater than 0.5 and often exceed 0.7, but they were only about 0.35 in AU87 and were effectively zero in AU88. The reason for the poor agreement during these autumns is not clear. It will be interesting to see whether such poor agreement is obtained in future autumns. The values of S involving the IERS data often lie well outside the quoted r.m.s. uncertainty for the IERS data by itself (which is between 0.12 and 0.25 ms); see particularly the values for SP88 and AU88. This implies either (i) that the r.m.s. difference between the ECMWF and UKMO evaluations is approximately half as large as the error in each evaluation, or (ii) that the r.m.s. error in the IERS data is at least a factor of two larger than the quoted value. The first alternative seems the more likely.

Assuming that the $\mathrm{DUT1}(t)$ data are more accurate than the $\mathrm{DUTA}(t)$ analyses, it is desirable to compare the meteorological forecasts of $\mathrm{DUTA}(t)$ with the $\mathrm{DUT1}(t)$ measurements. Such comparisons have the merit that errors in the determinations of the time series involved are not interrelated. This is not the case for the comparisons of the meteorological analyses and forecasts, of course, as the forecast fields provide the first-guess fields for the analyses. Five-day forecast values of $\mathrm{DUTA}(t)$ have been calculated according to the formula

$$\mathrm{DUTA}(t;5^*) = \Lambda_0 \int_{t-2.5}^{t+2.5} \chi_3(\tau;5^*)\,\mathrm{d}\tau. \tag{4.10}$$

(This formula is unlikely to give the best practical forecasts of $\mathrm{DUT1}(t)$, but was chosen to maintain as much continuity as possible with the presentation of §3.) Time series of $\Delta\mathrm{DUTA}(t;5^*)$, as defined from (3.2), (4.7) and (4.10), have been compared with $\Delta\mathrm{DUTA}(t;5)$ and $\Delta\mathrm{DUT1}(t;5)$ time series. Values of S and R^2 for the standard seasons are displayed in table 8 (cf. table 7). Generally speaking, the r.m.s. difference between the IERS data and meteorological analyses for a given season and centre is comparable with or greater than that between the meteorological centre's analyses and its forecasts. Not surprisingly, both of these are smaller than the r.m.s. difference between the IERS data and the meteorological forecasts. The main exceptions to these two statements occur in AU87 for ECMWF and SU87 and AU87 for UKMO when their forecasts agreed better with the IERS data than their analyses. The ECMWF model appears to perform slightly better than the UKMO model when compared with the IERS data. For example, the minimum seasonal value of R^2 for UKMO analysis and forecast comparisons in the two-year period, which is 0.58, is only exceeded by R^2 for the UKMO forecast and IERS data in two of the eight seasons. The corresponding minimum value of R^2 for ECMWF analysis and forecast comparisons (0.59) is exceeded by R^2 for the ECMWF forecast and IERS data in five of the eight seasons.

More clear-cut assessments of the AAM analyses and forecasts than have been possible here should result from the further improvements in geodetic measurement techniques which are expected to be achieved in the next few years.

Table 7. *Seasonal values of S and R^2 for combinations of 5* d *analysis changes in* DUTA(*t*), *according to UKMO or ECMWF, and in* DUT*1*(*t*), *according to IERS* (*see equations* (*3.4*) *and* (*3.5*))

season	IERS/ UKMO	IERS/ ECMWF	UKMO/ ECMWF
	values of S		
WI86–7	0.24	0.19	0.17
SP87	0.38	0.43	0.17
SU87	0.33	0.27	0.20
AU87	0.34	0.37	0.21
WI87–8	0.39	0.32	0.22
SP88	0.60	0.48	0.24
SU88	0.46	0.43	0.19
AU88	0.50	0.54	0.16
	values of R^2		
WI86–7	0.70	0.82	0.85
SP87	0.61	0.49	0.90
SU87	0.72	0.80	0.90
AU87	0.39	0.33	0.62
WI87–8	0.67	0.78	0.89
SP88	0.58	0.73	0.92
SU88	0.48	0.55	0.90
AU88	0.06	0.07	0.89

Table 8. *Seasonal values of S and R^2 for combinations of 5* d *analysis changes and 5* d *forecast changes in* DUTA(*t*) *or* DUT*1*(*t*)

season	IERS/ UKMO	IERS/ ECMWF	UKMO/ UKMO	ECMWF/ ECMWF
	values of S			
WI86–7	0.35	0.22	0.26	0.19
SP87	0.43	0.48	0.31	0.23
SU87	0.27	0.33	0.31	0.26
AU87	0.29	0.27	0.17	0.21
WI87–8	0.46	0.41	0.35	0.32
SP88	0.58	0.48	0.38	0.32
SU88	0.49	0.53	0.26	0.30
AU88	0.53	0.54	0.27	0.26
	values of R^2			
WI86–7	0.36	0.73	0.62	0.82
SP87	0.47	0.36	0.68	0.77
SU87	0.74	0.67	0.75	0.81
AU87	0.56	0.63	0.69	0.59
WI87–8	0.51	0.65	0.70	0.77
SP88	0.66	0.75	0.81	0.89
SU88	0.36	0.30	0.82	0.75
AU88	0.00	0.05	0.58	0.72

5. Forecasts of the equatorial components

Brzezinski's (1987) study of the contributions to the equatorial components by the matter terms revealed persistent though irregularly modulated oscillations with periods of between 9 d and 13 d. As suggested by Eubanks *et al.* (1988), these oscillations are manifestations of one of the gravest 'equivalent barotropic' linear Rossby waves investigated by Longuet-Higgins (1968) (see also Chapman & Lindzen

PHILOSOPHICAL TRANSACTIONS OF THE ROYAL SOCIETY A MATHEMATICAL, PHYSICAL & ENGINEERING SCIENCES

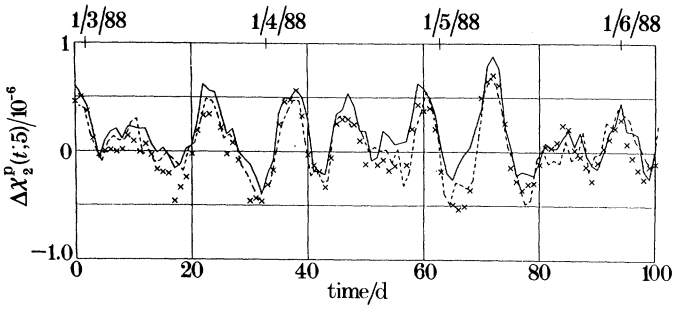

Figure 13. Time series of $\Delta\chi_2^p(t;5)$ based on UKMO 00Z analyses from March 1987 to June 1987 (crosses) and $\Delta\chi_2^p(t;5^*)$ based on 5 d forecasts from UKMO (full line) and ECMWF (dashed line), see equations (2.1)–(2.3), (3.1) and (3.2). Bottom axis is day after 1 January 1975 (day zero) minus 4735.

1970). Madden's (1979) calculations of the periods of the Rossby waves for conditions representative of the Earth's atmosphere (i.e., 'equivalent depths' between 8 and 12 km) show that the mode of degree 3 and order 1, which contains the largest contributions to the matter term $\boldsymbol{\chi}^p$, has a period of between 8 and 9 d. This mode must exchange angular momentum with the Earth through surface pressure torques with the same period. The main torque arises from the surface pressure on the Earth's equatorial bulge. As discussed in Appendix C, this torque happens to be represented accurately by the standard tidal equations for a sphere because the neglect of the Earth's equatorial bulge in these equations is exactly compensated by the neglect of centripetal acceleration!

These surface torques are associated with such large horizontal scales that, in spite of their irregular temporal modulation, they might be expected to be well represented in the numerical forecast models and data assimilation systems. Indeed determinations of the matter term $\boldsymbol{\chi}^p$ using ECMWF, JMA, NMC and UKMO data over the period 1980–1986 have been found to be in close agreement (Eubanks *et al.* (1988); Bell & Nitsas (1989)). Figure 13 displays the 5 d forecast changes of χ_2^p made by the UKMO (continuous line) and ECMWF (dashed line) and the UKMO five-day analysis changes (crosses) during SP88. Clearly the forecast models capture the oscillations quite accurately. Table 9 shows that the performance of the forecast models during this period is representative of that of both models for χ_1^p and χ_2^p during all the periods investigated (with the exception of SU88), the correlation coefficient R^2 being consistently close to 0.75. The performances of the two models for these terms are very similar. Neither model has in its forecasts a noticeable tendency to underestimate the amplitude of the fluctuations in χ_1^p or χ_2^p, the regression slope G consistently lying between 0.9 and 1.1.

The wind term contributions to χ_1 and χ_2 are somewhat smaller in magnitude than those of the matter terms χ_1^p and χ_2^p. Comparisons of evaluations of the wind terms similar to those for the matter terms display no day to day agreement but T. M. Eubanks (personal communications), by comparing NMC data at 00Z and 12Z, discovered a diurnal variation in χ_2^w which has a seasonal modulation. Evaluations of χ_2^w at 00Z and 12Z from (*a*) ECMWF and (*b*) UKMO data for 1988 are displayed in figure 14. For clarity of presentation, all the values shown in figures 14–16 are 11 d running means. The ECMWF data in figure 14 are uninitialized analyses. A seasonally modulated diurnal variation is clearly apparent in the data from both centres. χ_2^w (12Z) − χ_2^w(00Z) for ECMWF data is a maximum in the NH summer and

PHILOSOPHICAL TRANSACTIONS OF THE ROYAL SOCIETY A MATHEMATICAL, PHYSICAL & ENGINEERING SCIENCES

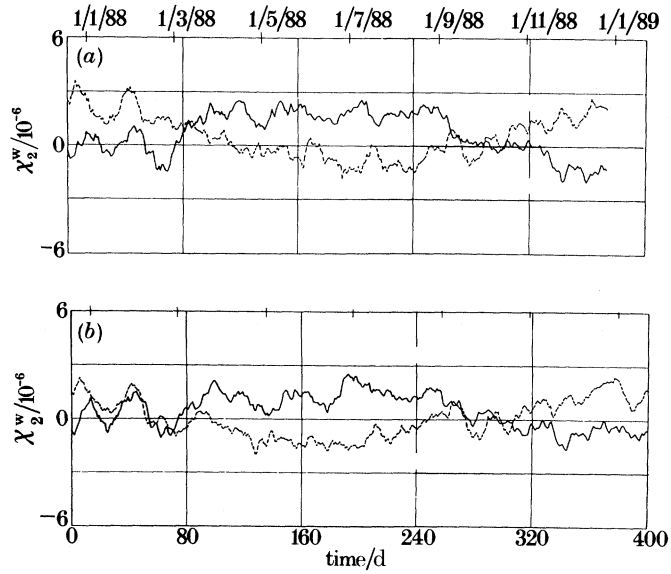

Figure 14. Time series of the analyses of χ_2^w made by (*a*) ECMWF and (*b*) UKMO. The full curves display analyses valid at 00Z and the dashed curves analyses valid at 12Z. The ECMWF data presented here are uninitialized. All data have been subjected to an 11 d running mean filter. Bottom axes are day after 1 January 1975 (day zero) minus 4735.

Table 9. *Seasonal values of* R^2 *and* G *for 5* d *forecast changes in* χ_1^p *and* χ_2^p *made by UKMO and ECMWF*

	χ_1^p		χ_2^p	
	UKMO	ECMWF	UKMO	ECMWF
	values of R^2			
WI86–7	0.67	0.70	0.73	0.74
SP87	0.77	0.77	0.70	0.74
SU87	0.70	0.61	0.67	0.77
AU87	0.86	0.87	0.84	0.85
WI87–8	0.82	0.85	0.71	0.78
SP88	0.79	0.78	0.84	0.82
SU88	0.67	0.64	0.45	0.60
AU88	0.81	0.75	0.70	0.78
	values of G			
WI86–7	1.02	1.07	0.84	0.91
SP87	1.05	1.02	0.99	0.91
SU87	0.92	0.97	0.87	0.91
AU87	0.92	0.91	0.97	0.99
WI87–8	1.02	0.98	0.97	1.03
SP88	0.96	0.98	0.92	0.94
SU88	0.87	0.92	1.04	0.98
AU88	0.92	0.96	1.01	1.01

has a peak minus trough seasonal amplitude of nearly 6×10^{-7} (non-dimensional units). The same quantity for UKMO data has a similar phase but somewhat smaller amplitude.

Bell & Nitsas (1989) and Bell & White (1991) discuss diurnal variations in $\boldsymbol{\chi}^w$ due to heating of the atmosphere produced by insolation. The oscillatory spatial pattern

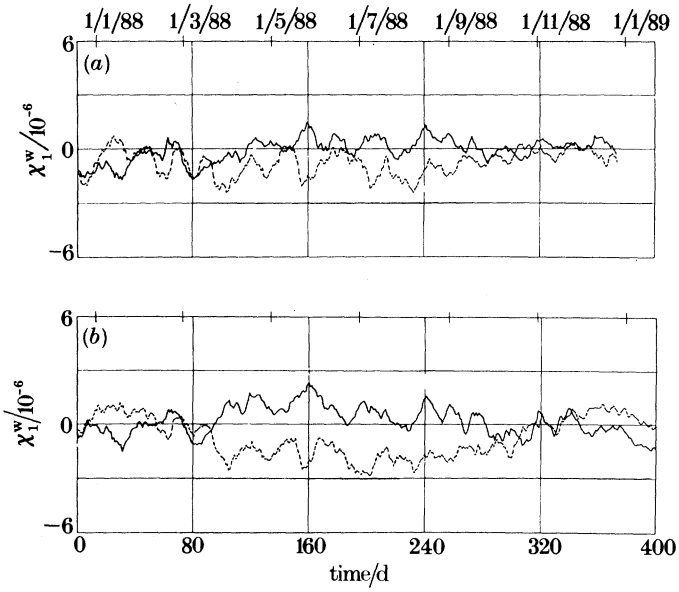

Figure 15. As for figure 14 except that analyses are of χ_1^w.

of the variations follows the Sun, so their angular momentum is stationary in any inertial frame. The variations are forced by the $P_2^1(\sin\phi)\exp i\lambda$ component of the diurnal heating and consequently have a seasonal modulation. Lindzen (1965), who pointed out that this component of the heating is orthogonal to all the Hough functions with a diurnal period, derived expressions for the induced velocity field. The resulting seasonal oscillation in $\chi_2^w(12Z)-\chi_2^w(00Z)$ is shown by Bell & White (1991) to have the same phase as that implied by the data in figure 14 and a peak minus trough amplitude of 4×10^{-7}.

The thermally forced χ_1^w oscillation has maxima and minima at 06Z and 18Z and hence no signal at 00Z and 12Z. Evaluations of χ_1^w at 00Z and 12Z by (*a*) ECMWF (from uninitialized data) and (*b*) UKMO are presented in figure 15. Only a weak seasonally modulated diurnal oscillation is apparent in the ECMWF data, but one is clearly present in the UKMO data with an amplitude comparable with that of the χ_2^w variation in figure 14*b*. This clear discrepancy between (*a*) UKMO data on the one hand and (*b*) the ECMWF (and NMC) data and the thermally forced Rossby-wave calculations on the other hand, merits further investigation. Investigation of data valid at 06Z and 18Z would clearly also be desirable.

Figure 16 presents 48 h and 60 h forecasts of χ_2^w made by ECMWF starting from 12Z analyses. Comparison of this figure with figure 14*a* shows that the seasonally modulated diurnal variation has a larger magnitude in 2 d forecasts than the analysis data. The present initialization step, which is designed to retain diabatically-forced waves (Wergen 1989), had negligible impact on the 1988 χ_1^w and χ_2^w data (graphs not shown) and so appears not to be responsible for the discrepancy between analyses and forecasts. The forced Rossby-wave analysis suggests that an enhanced diurnal variation in the diabatic heating during the first two or three days of the forecast could be responsible. Alternatively, the analysis systems may be unable to separate the diurnal cycle from the 'noise' in the χ^w data. The vigorous seasonal variation of figure 16 appears to be maintained in the 10 d forecast (figures not shown).

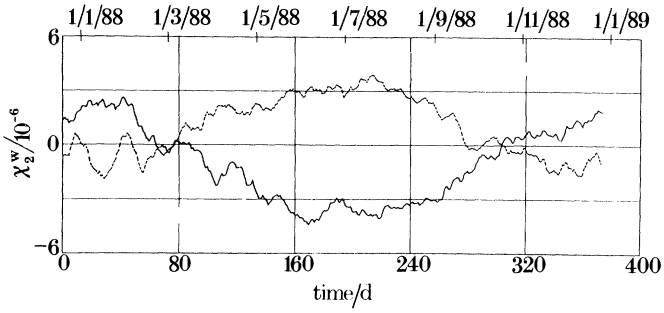

Figure 16. Forecast time series of χ_2^w produced by the ECMWF forecast system from 12Z start times. The full line presents the 48 h forecasts and the dashed line 60 h forecasts. All data have been subjected to an 11 d running mean filter. Bottom axis as for figures 14 and 15.

6. Concluding remarks

Several of the findings of the present investigation deserve further study. Seasonally averaged biases of the UKMO 5 d forecasts in 1987 and 1988 of χ_3, the axial component of AAM, were quite different despite the similarity of the observational databases used and the fact that the forecast system underwent only minor changes during this period. The 10 d ECMWF forecasts exhibited considerable 'skill' in some seasons (e.g., spring 1988) but not in others (e.g. spring 1987). The extent to which these results are manifestations of slow changes in flow régime in the atmosphere over the two-year period could be established by appropriate diagnostic calculations involving the influence on the analysis fields of data sparse regions.

Five-day forecast changes of χ_3 were found to be systematically smaller in amplitude than the analysis changes for both the UKMO and ECMWF GNWP models, particularly for the UKMO model. Moreover, the correlation between analysis and forecast changes of χ_3 was greatest for forecasts out to 3 or 4 d. The slow 'decay' of forecast skill with forecast lead-time would be consistent with large-scale (i.e. low wavenumber) modes of motion in the atmosphere being largely responsible for the net torque acting on the underlying planet and motions associated with smaller horizontal scales (higher wavenumber) playing a comparatively minor role in the angular momentum transfer process. The comparatively poor correlation between the 1 d forecast and analysis changes is probably largely due to the difficulty of analysing small changes in AAM from available data.

So far as changes in the dimensionless measure $\boldsymbol{\chi}$ of the equatorial component of H_i are concerned, worthy of note is the high quality of 5 d forecasts from both UKMO and ECMWF of the 'matter' contribution $\boldsymbol{\chi}^p$ to $\boldsymbol{\chi}$ (see equation (2.1)), fluctuations in which include a pronounced oscillation with a period of about 10 d (see §5 and Appendix C). Determinations of the seasonal modulation of the observed diurnal changes in the wind contributions $\boldsymbol{\chi}^w$ to $\boldsymbol{\chi}$ are less accurate. Analyses based on the UKMO model of the differences between χ_1^w at Greenwich midnight 00Z and noon 12Z contain variations which are almost certainly spurious (see §5). The ECMWF 2 d and $2\frac{1}{2}$ d forecasts of the 00Z minus 12Z differences in χ_2^w have twice the amplitude of the corresponding analysis differences. Improvements in the geographical coverage of the meteorological data and in their assimilation into the models and/or better parametrizations of diabatic heat fluxes will be needed to remove these discrepancies in future analyses and forecasts.

Routine determinations of all three components of AAM are now being made at several meteorological centres, under a programme to be coordinated in the future by the Sub-Bureau for Atmospheric Angular Momentum (based at the NMC in Washington) of the IERS. A development programme is currently in hand to facilitate the effective use of the AAM data so produced and disseminated to meteorologists, geodesists and others interested in the wide range of dynamical processes involved. To make the best use of AAM time series in meteorological research it will be necessary to incorporate AAM studies into wider diagnostic studies of the processes underlying global atmospheric circulation. To this end, an important step would be the routine production of time series of fluctuations in topographic and boundary layer stresses at the Earth's surface and the corresponding time series of $L_i(t)$, the net torque.

We are especially grateful to Miss W. L. Adams, Dr B. R. Barwell, Dr R. A. Bromley, Dr A. J. Gadd, Mr C. D. Hall, Mr P. J. Trevelyan and Dr A. A. White of the UKMO and Dr K. Arpe, Dr D. M. Burridge, Dr A. Hollingsworth and Dr A. J. Simmons of the ECMWF for helpful comments and other assistance throughout the course of this work.

Appendix A. Fluctuations in the Earth's rotation

Fluctuations in the rotation vector ω_i of the solid Earth (see equation (1.3)) are caused by: (*a*) agencies that change the inertia tensor I_{ij} of the solid Earth, and (*b*) applied torques. Contributions to the former include (i) deformations of the solid Earth produced by the gravitational action of the Moon, Sun and other astronomical bodies (periodic Earth tides) and also non-periodic variable surface stresses associated with fluid flow in the underlying liquid metallic core and the overlying hydrosphere and atmosphere, as well as (ii) mass redistribution associated with earthquakes, melting of ice, and, on geological timescales, mantle convection and movement of tectonic plates. As to the applied torques, the gravitational action of the Moon, etc. on the Earth's tidal bulge is sufficient to retard the speed of rotation of the Earth at a rate corresponding to a gradual lengthening of the day by about 10^{-3} seconds per century. Somewhat larger torques which fluctuate irregularly in magnitude and sign on timescales upwards of a few years are produced by core motions, which geophysicists have argued on general grounds to be responsible for the so-called 'decadal' changes in the length of day (LOD) (see equation (1.6)) of up to 5×10^{-3} s in amplitude and associated polar motion. As noted in §1, the strongest torques acting on the solid Earth are those produced by atmospheric motions. Fluctuations in the atmospheric 'super-rotation' (see figure 2) can generate irregular changes in the LOD of up to about 0.5×10^{-3} s on timescales as short as a few days; fluctuations in non-axisymmetric features of the pressure and wind fields can produce displacements of the pole of rotation of several metres. (For references see Munk & Macdonald 1960; Lambeck 1980; Hide 1977, 1984, 1986, 1989; Rochester 1984; Cazenave 1986; Wahr 1986, 1988; Moritz & Mueller 1987; Jault *et al.* 1988.)

Determinations of $\Lambda(t)$ and $\boldsymbol{m}(t)$ (see equation (1.6)) are nowadays made by positional astronomers under a co-operative programme of the International Astronomical Union (IAU) and the International Association of Geodesy (IAG) of the International Union of Geodesy and Geophysics (IUGG), which operate the International Earth Rotation Service (IERS) based in Paris. Modern methods for monitoring the Earth's rotation are based on positional observations of distant

quasars using the very long baseline interferometry (VLBI) technique of radio astronomy and of artificial satellites or corner reflectors placed on the Moon using the technique of laser ranging (i.e. SLR and LLR). (For references see Moritz & Mueller 1987.) The observational time series of $A(t)$ and $\boldsymbol{m}(t)$ can, by appropriate filtering techniques, be separated into four components, namely irregular (i.e., chaotic or non-periodic) variations (*a*) on 'decadal' timescales and (*b*) on interannual, seasonal, intraseasonal and shorter timescales (including the chandlerian free wobble with period 435 d and irregularly varying amplitude and phase) together with (*c*) periodic 'tidal' variations, and (*d*) long-term trends.

Thanks to advances in meteorological data acquisition and processing methods, starting with the First GARP Global Experiment (FGGE) of the Global Atmospheric Research Programme (GARP) organized by the International Council of Scientific Unions (ICSU) and the World Meteorological Organization (WMO), and to improved techniques for monitoring the Earth's rotation (as outlined above), there is now overwhelming evidence that short-term irregular changes in the Earth's rotation speed can be accounted for without having to invoke substantial non-meteorological contributions to the angular momentum budget (Hide *et al.* 1980; BHWW; Rosen & Salstein 1983, 1985; Rosen *et al.* 1987; Morgan *et al.* 1985; Dickey *et al.* 1986, 1990), see figure 3. One consequence of this important finding is that the time series can be used on appropriate timescales as proxy meteorological data sets (see, for example, Feissel & Gambis 1980; Langley *et al.* 1981; Eubanks *et al.* 1985; Cooper *et al.* 1989; Chao 1988). It has thus been established, for example, that the global atmospheric super-rotation fluctuates not only on seasonal and interannual timescales but also irregularly but persistently on timescales ranging from about 30 to 80 d (see also Madden & Julian 1972). This irregular 'intraseasonal' fluctuation, which is of great intrinsic scientific interest and also of potential practical significance in long-range weather forecasting, is now being studied intensively by theoretical and observational research groups throughout the world (for references see Benzi *et al.* 1986; Emanuel 1987; Ghil & Childress 1987; Haarsma & Opsteegh 1988; Knutson & Weickmann 1987; Legras & Ghil 1985; Madden 1986; Reinhold 1987; Simmons *et al.* 1983; Vautard *et al.* 1988; Wang 1988).

The present study was undertaken as part of a much wider programme of research on atmospheric excitation of changes in the Earth's rotation started over a decade ago, which has various ramifications in meteorology, oceanography, geodesy and geophysics. In 1983, responding to some of the above-mentioned developments, the IAG of the IUGG set up a special working group charged with the task of promoting basic and applied research on these ramifications (see Dickey *et al.* 1986; Hide 1984). One of the initiatives taken by the working group was to urge suitably equipped meteorological centres to forecast changes in all three components of AAM out to several days from the outputs of reliable GNWP models. In addition to routine AAM analyses (see BHWW, Hide 1984; Morgan *et al.* 1985; Rosen & Salstein 1985; Dickey *et al.* 1986; Bell & Whysall 1987; Naito *et al.* 1987; Rosen *et al.* 1987*a*; Risbey & Stone 1988; Bell & Nitsas 1989), forecasts are now produced by four centres: the U.K. Meteorological Office (UKMO), the European Centre for Medium Range Weather Forecasts (ECMWF), the U.S. National Meteorological Center (USNMC), and the Japanese Meteorological Agency (JMA). Rosen *et al.* (1987*b*) have already analysed forecasts of the wind contribution to the axial component of AAM (see equation (2.3)) based on the GNWP model in operational use at the USNMC, with encouraging results.

PHILOSOPHICAL TRANSACTIONS OF THE ROYAL SOCIETY A MATHEMATICAL, PHYSICAL & ENGINEERING SCIENCES

We note here in passing that by the mid-1970s it was becoming evident that progress then being made by geodesists with the monitoring of the Earth's rotation and by meteorologists with the development of GNWP models was almost bound to lead in due course to the close co-operation that is now occurring. But it was also clear that the first GNWP models, then quite new, were not up to the task of providing useful AAM forecasts. The inadequate representation of dynamical effects due to orography was initially one of several sources of uncertainty in all GNWP models, in some of which the super-rotation increased steadily with time, in disagreement with both observations and the physical laws governing angular momentum. Better parametrization of orographic drag and other modifications have been made to GNWP models in recent years, producing evident improvements (at least in the case of the models used in the present study) in the treatment of angular momentum fluctuations.

Fluctuations in the equatorial components of AAM contribute to the observed 'polar motion' of the Earth's figure axis relative to its rotation axis, including the chandlerian wobble at the 'free' period of 435 d, which exhibits irregular modulations in amplitude (see §2). The hypothesis that meteorological processes make a substantial contribution to the wobble has had a chequered history since it was first advanced around the beginning of the century, not long after the wobble was discovered from determinations of temporal variations in the latitude of various astronomical observatories (see Munk & Macdonald 1960; Wilson & Haubrich 1976; Lambeck 1980; Wahr 1983; Moritz & Mueller 1987; Groten & Lenhardt 1988). The hypothesis has not yet been tested fully, for even with modern meteorological data sets equatorial AAM fluctuations cannot yet be determined as accurately as can those occurring in the axial component, and there are complications associated with uncertainties in: (*a*) how to allow for the response of the oceans, and (*b*) the nature of the processes that damp the wobble (see BHWW; Hide 1984, 1985; Cazenave 1986; Brzezinski 1987; Eubanks *et al.* 1988; Vondrák & Pejović 1988). Relationships between $\boldsymbol{m}(t)$ and the excitation function $\boldsymbol{\chi}(t)$ can be obtained by solving equation (2.6) to give

$$\boldsymbol{m}(t) = \boldsymbol{m}(t_0)\,\mathrm{e}^{\mathrm{i}\sigma(t-t_0)} - \sigma\Omega^{-1}\{\boldsymbol{\chi}(t) - \boldsymbol{\chi}(t_0)\,\mathrm{e}^{\mathrm{i}\sigma(t-t_0)}\} - \mathrm{i}\sigma(1+\sigma\Omega^{-1})\,\mathrm{e}^{\mathrm{i}\sigma t}\int_{t_0}^{t}\boldsymbol{\chi}(\tau)\,\mathrm{e}^{-\mathrm{i}\sigma\tau}\,\mathrm{d}\tau, \tag{A 1}$$

or

$$\boldsymbol{\chi}(t) = \boldsymbol{\chi}(t_0)\,\mathrm{e}^{-\mathrm{i}\Omega(t-t_0)} - \Omega\sigma^{-1}\{\boldsymbol{m}(t) - \boldsymbol{m}(t_0)\,\mathrm{e}^{-\mathrm{i}\Omega(t-t_0)}\} + \mathrm{i}\Omega(1+\Omega\sigma^{-1})\,\mathrm{e}^{-\mathrm{i}\Omega t}\int_{t_0}^{t}\boldsymbol{m}(\tau)\,\mathrm{e}^{\mathrm{i}\Omega\tau}\,\mathrm{d}\tau. \tag{A 2}$$

Appendix B. Fluctuations in the zonal kinetic energy of the atmosphere

To estimate the order of magnitude of the temporal fluctuations in kinetic energy associated with the 'super-rotation' of the atmosphere that accompany the observed fluctuations in the axial component of AAM, we consider the behaviour of the simplest imaginable system, namely one consisting of concentric spherical shells α and β (the 'solid Earth' and the 'atmosphere' respectively) of fixed moments of inertia I_α and I_β rotating about a common axis through their centre with temporally-variable angular speeds Ω_α and Ω_β.

Associated with the relative angular motion $(\Omega_\beta - \Omega_\alpha)$ of the outer to the inner shell are the 'relative angular momentum'

$$\mathscr{H} \equiv I_\beta(\Omega_\beta - \Omega_\alpha) \tag{B 1}$$

and concomitant kinetic energy

$$\mathscr{E} \equiv \tfrac{1}{2} I_\beta(\Omega_\beta - \Omega_\alpha)^2. \tag{B 2}$$

It follows from these equations that fractional changes in $\mathscr{E}$ are twice those in $\mathscr{H}$, for

$$\mathscr{H}^{-1}\dot{\mathscr{H}} = (\Omega_\beta - \Omega_\alpha)^{-1}(\dot{\Omega}_\beta - \dot{\Omega}_\alpha) = \tfrac{1}{2}\mathscr{E}^{-1}\dot{\mathscr{E}}. \tag{B 3}$$

In the absence of external torques, the total angular momentum of the system $I_\alpha \Omega_\alpha + I_\beta \Omega_\beta$ remains fixed, so that

$$I_\alpha \dot{\Omega}_\alpha + I_\beta \dot{\Omega}_\beta = 0. \tag{B 4}$$

But concomitant fluctuations in the total kinetic energy of the system $\mathscr{E}_\alpha + \mathscr{E}_\beta$ (say), where

$$\mathscr{E}_\alpha \equiv \tfrac{1}{2} I_\alpha \Omega_\alpha^2 \quad \text{and} \quad \mathscr{E}_\beta \equiv \tfrac{1}{2} I_\beta \Omega_\beta^2, \tag{B 5}$$

are non-zero except in the special case when $\Omega_\beta = \Omega_\alpha$, corresponding to the state of minimum total kinetic energy for given total angular momentum. This follows from equations (B 4) and (B 5), which give

$$\dot{\mathscr{E}}_\alpha = I_\alpha \Omega_\alpha \dot{\Omega}_\alpha = -I_\beta \Omega_\alpha \dot{\Omega}_\beta, \tag{B 6}$$

$$\dot{\mathscr{E}}_\beta = I_\beta \Omega_\beta \dot{\Omega}_\beta = -I_\alpha \Omega_\beta \dot{\Omega}_\alpha, \tag{B 7}$$

so that

$$\dot{\mathscr{E}}_\alpha + \dot{\mathscr{E}}_\beta = (\Omega_\alpha - \Omega_\beta) I_\alpha \dot{\Omega}_\alpha = (\Omega_\beta - \Omega_\alpha) I_\beta \dot{\Omega}_\beta. \tag{B 8}$$

Finally, we note that

$$\mathscr{E}_\alpha^{-1}\dot{\mathscr{E}}_\alpha / \mathscr{E}_\beta^{-1}\dot{\mathscr{E}}_\beta = -I_\beta \Omega_\beta / I_\alpha \Omega_\alpha. \tag{B 9}$$

Since $I_\beta / I_\alpha \approx 10^{-6}$ and $\Omega_\beta / \Omega_\alpha \approx 1$, proportionate kinetic energy fluctuations of the atmosphere greatly exceed those of the solid Earth.

A more refined model could be considered in which the outer shell β was divided into regions rotating with different angular speeds, to represent horizontal and vertical variations of wind speed. But the essential conclusion would not be changed, namely that the observed fluctuations in AAM are indicative of substantial fluctuations in zonal kinetic energy associated with atmospheric motions. Underlying these fluctuations in zonal kinetic energy are energy conversion and distribution processes involving interactions of the non-zonal components of the wind field with the non-zonal and zonal components and also with the density fields produced and maintained by differential solar heating. It is of course the potential energy due to the action of gravity on that density field that provides the ultimate source of the kinetic energy of atmospheric motions.

Appendix C. The torque on the Earth's bulge

At first sight it might seem surprising that a numerical atmospheric model based on a spherical coordinate system which does not explicitly represent the Earth's equatorial bulge in the formulation of the surface boundary conditions can be used

to determine changes in the equatorial component of AAM brought about largely by pressure torques acting on the bulge.

The surface pressure torque on the Earth's bulge is most easily calculated by transforming the equations of motion from spherical coordinates (r, θ, λ) (θ being co-latitude and λ longitude) into spheroidal coordinates, defined by

$$r' = r - \Omega^2 r^2 \sin^2\theta/2g, \quad \theta' = \theta, \quad \lambda' = \lambda, \tag{C 1}$$

which follow equipotential surfaces. The meridional pressure gradient $\partial p/\partial\theta$ then transforms to

$$\frac{\partial p}{\partial \theta} = \frac{\partial p}{\partial \theta'} + \left(\frac{\partial r'}{\partial \theta}\right)\left(\frac{\partial p}{\partial r'}\right)$$

$$= \partial p/\partial\theta' - (\Omega^2 r^2 \sin\theta\cos\theta/g)\,\partial p/\partial r'. \tag{C 2}$$

The pressure torque on the atmosphere is

$$\boldsymbol{L}^{\mathrm{p}} \equiv \iiint [(\partial p/\partial\theta)(-\hat{\boldsymbol{x}}_1 \sin\lambda + \hat{\boldsymbol{x}}_2 \cos\lambda) - (\partial p/\partial\lambda)(\hat{\boldsymbol{x}}_1 \cos\lambda + \hat{\boldsymbol{x}}_2 \sin\lambda)]\,\mathrm{d}\,(\text{volume}), \tag{C 3}$$

where $\hat{\boldsymbol{x}}_1$ and $\hat{\boldsymbol{x}}_2$ are unit vectors in the equatorial plane as indicated in figure 1. Using the shallow atmosphere approximation, $\boldsymbol{L}^{\mathrm{p}}$ is easily shown to reduce to

$$\boldsymbol{L}^{\mathrm{p}} = \int_0^{2\pi}\int_0^{\pi} g^{-1}\Omega^2 \bar{R}^4 p_{\mathrm{s}} \sin\theta\cos\theta\,(\hat{\boldsymbol{x}}_1 \sin\lambda - \hat{\boldsymbol{x}}_2 \cos\lambda)\sin\theta\,\mathrm{d}\theta\,\mathrm{d}\lambda, \tag{C 4}$$

the other pressure gradient terms cancelling after integration by parts.

The linearized meridional equation of motion in spherical coordinates is

$$\rho(\partial v/\partial t + 2\Omega u\cos\theta + \Omega^2 r\cos\theta\sin\theta) = -r^{-1}\,\partial p/\partial\theta. \tag{C 5}$$

On transforming to the spheroidal coordinates defined above and using the hydrostatic approximation ($\partial p/\partial r' = -\rho g$), the centripetal acceleration term is cancelled by the second term on the right-hand side of equation (C 2). In consequence, the standard tidal equations for a sphere, in which the centripetal term is neglected, satisfactorily represent the surface pressure torque on the equatorial bulge (as verified in greater detail in Bell & Nitsas (1989) and Bell & White (1991)).

References

Arpe, K., Hollingsworth, A., Lorenc, A. C., Tracton, M. S., Uppala, S. & Kallberg, P. 1985 The response of numerical weather prediction systems to FGGE II-b data, Part II: Forecast verifications and implications for predictability. *Q. Jl R. met. Soc.* **111**, 67–102.

Arpe, K. & Klinker, E. 1986 Systematic errors in the ECMWF operational model in mid-latitudes. *Q. Jl R. met. Soc.* **112**, 181–202.

Barnes, R. T. H., Hide, R., White, A. A. & Wilson, C. A. 1983 Atmospheric angular momentum fluctuations, length of day changes and polar motion. *Proc. R. Soc. Lond.* A **387**, 31–73.

Bell, M. J. & Nitsas, S. 1989 *An intercomparison of four sets of angular momentum data and a discussion of the equatorial components.* Met O 13 Branch Memorandum 173. UKMO.

Bell, M. J. & White, A. A. 1991 Some aspects of the dynamics of the equatorial components of atmospheric angular momentum. (In preparation.)

PHILOSOPHICAL TRANSACTIONS OF THE ROYAL SOCIETY A MATHEMATICAL, PHYSICAL & ENGINEERING SCIENCES

Bell, M. J. & Whysall, K. D. B. 1987 *Atmospheric angular momentum fluctuations and changes in the Earth's rotation: Meteorological Office users' guide to data sets and codes.* Met O 21 Internal Report IR87/3.

Bell, R. S. & Dickinson, A. 1987 *The Meteorological Office operational numerical weather prediction system.* Meteorological Office Scientific Paper no. 41, pp. viii, 61.

Bengtsson, L., Ghil, M. & Källen, E. (eds) 1981 Dynamic meteorology: data assimilation methods. Applied mathematical Sciences, vol. 36. Springer Verlag. pp. x, 330.

Bengtsson, L., Kanamitsu, M., Kållberg, P. & Uppala, S. 1982 FGGE 4-dimensional data assimilation at ECMWF. *Bull. Am. Meteorol. Soc.* **69**, 29–43.

Benzi, R., Saltzman, B. & Wiin-Nielsen, A. C. (eds) 1986 *Anomalous atmospheric flows and blocking. Adv. Geophys.* **29**, pp. xvi, 459.

Bongers, T. & Wyrtki, K. 1987 Sea level at Tahiti – a minimum of variability. *J. phys. Oceanogr.* **17**, 164–168.

Brzezinski, A. 1987 Statistical investigations on atmospheric angular momentum functions and their effects on polar motion. *Manuscr. Geodaetica* **12**, 268–281.

Bureau International de l'Heure 1987 Annual Report for 1986 (ed. M. Feissel). Observatoire de Paris.

Caplan, P. M. & White, G. H. 1989 Performance of the National Meteorological Center's medium-range model. *Weather Forecasting* **4**, 391–400.

Carton, J. A. & Wahr, J. M. 1986 Modelling the pole tide and its effect on the Earth's rotation. *Geophys. Jl R. astr. Soc.* **84**, 121–137.

Cazenave, A. (ed.) 1986 *Earth rotation: solved and unsolved problems*, pp. xiv, 330. Dordrecht: Reidel.

Chao, B. F. 1988 Correlation of interannual length-of-day variation with El Niño – Southern Oscillation, 1972–1986. *J. geophys. Res.* **93**, 7709–7715.

Chapman, S. & Lindzen, R. S. 1970 *Atmospheric tides; thermal and gravitational.* Dordrecht: Reidel.

Cooper, N. S., Whysall, K. D. B. & Bigg, G. R. 1989 Recent decadal climate variations in the tropical Pacific. *Int. J. Climatol.* **9**, 221–242.

Daley, R. 1981 Normal mode initialization. In *Dynamic meteorology; data assimilation methods* (ed. L. Bengtsson *et al.*), pp. 77–109. Applied Mathematical Sciences, vol. 36. Springer-Verlag.

Dickey, J. O., Eubanks, J. M. & Hide, R. 1990 Interannual and decadal fluctuations of the Earth's rotation. *Geophys. Monographs. Amer. Geophys. Un.* **59**, 157–162.

Dickey, J. O., Eubanks, T. M. & Steppe, J. A. 1986 High accuracy Earth rotation and atmospheric angular momentum measurements. In *Earth rotation: solved and unsolved problems* (ed. A. Cazanave), pp. 137–162. Dordrecht: Reidel.

Emanuel, K. 1987 An air–sea interaction model of intraseasonal oscillations in the tropics. *J. atmos. Sci.* **44**, 2324–2340.

Eubanks, T. M., Steppe, J. A., Dickey, J. O. & Callaham, P. S. 1985 A spectral analysis of the Earth's angular momentum budget. *J. geophys. Res.* **90**, 5385–5404.

Eubanks, T. M., Steppe, J. A., Dickey, J. O., Rosen, R. D. & Salstein, D. A. 1988 Causes of rapid motions of the Earth's pole. *Nature, Lond.* **334**, 115–119.

Feissel, M. & Gambis, D. 1980 La mise en évidence de variations rapides de la durée du jour. *C. r. hebd. Séanc. Acad. Sci., Paris* B **291**, 271–273.

Ghil, M. & Childress, S. 1987 *Topics in geophysical fluid dynamics: atmospheric dynamics, dynamo theory and climate dynamics*, pp. xv, 485. New York: Springer Verlag.

Groten, E. & Lenhardt, H. 1988 Some general considerations on new aspects of Chandler motion. *Allg. Vermess. Nachr. Kahlsruhe (Int. Edn)* **5**, 18–26.

Haarsma, R. J. & Opsteegh, J. D. 1988 Barotropic instability of planetary-scale flows. *J. atmos. Sci.* **45**, 2789–2810.

Hide, R. 1977 Towards a theory of irregular variations in the length of the day and core-mantle coupling. *Phil. Trans. R. Soc. Lond.* A **284**, 547–554.

Hide, R. 1984 Rotation of the atmospheres of the Earth and planets. *Phil. Trans. R. Soc. Lond.* A **313**, 107–121.

PHILOSOPHICAL TRANSACTIONS OF THE ROYAL SOCIETY A MATHEMATICAL, PHYSICAL & ENGINEERING SCIENCES

Hide, R. 1985 On the excitation of short-term variations in the length of the day and polar motion. *Geophys. Surv.* **7**, 163–167.

Hide, R. 1986 Presidential address – the Earth's differential rotation. *Q. Jl R. astr. Soc.* **278**, 3–14.

Hide, R. 1988 Forecasting short-term changes in the Earth's rotation. In *The Earth's rotation and reference frames for geodesy and geodynamics* (ed. A. K. Babcock & G. A. Wilkins), pp. 287–288. I.A.U. Publication.

Hide, R. 1989 Fluctuations in the Earth's rotation and the topography of the core-mantle interface. *Phil. Trans. R. Soc. Lond.* A **328**, 351–363.

Hide, R. 1990 Forecasting short-term changes in the Earth's rotation using global numerical weather prediction models. *Geophys. Monographs Am. Geophys. Un.* **59**, 145–146.

Hide, R., Birch, N. T., Morrison, L. V., Shea, D. J. & White, A. A. 1980 Atmospheric angular momentum fluctuations and changes in the length of the day. *Nature, Lond.* **286**, 114–117.

Hollingsworth, A. 1987 Objective analysis for numerical weather prediction. In *Short and medium-range numerical weather prediction* (ed. T. Matsuno), pp. 11–60. Tokyo: Meteorological Society of Japan.

Hollingsworth, A., Lorenc, A. C., Tracton, M. S., Arpe, K., Cats, G., Uppala, S. & Kallberg, P. 1985 The response of numerical weather prediction systems to FGGE level IIb data. Part I: Analyses. *Q. Jl R. met. Soc.* **111**, 1–67.

Hollingsworth, A., Shaw, D. B., Lönnberg, P., Illari, L., Arpe, K. & Simmons, A. J. 1986 Monitoring of observation and analysis quality by a data assimilation system. *Mon. Weather Rev.* **114**, 861–879.

Jarraud, M., Simmons, A. J. & Kanamitsu, M. 1988 Sensitivity of medium range weather forecasts to the use of an envelope orography. *Q. Jl R. met. Soc.* **114**, 989–1026.

Jault, D., Gire, C. & Le Mouël 1988 Westward drift, core motions and the exchange of angular momentum between core and mantle. *Nature, Lond.* **333**, 353–356.

Kendall, Sir M. G. & Stuart, A. 1977 *The advanced theory of statistics, vol. 1: distribution theory.* 4th edn. Griffin (xii + 472 pages.).

Klinker, E. & Sardeshmukh, P. D. 1988 The diagnosis of systematic errors in numerical weather prediction models. In *ECMWF Workshop on diabatic forcing*, pp. 209–244. European Centre for Medium Range Weather Forecasts (Shinfield, Reading) Publication.

Knutson, T. R. & Weickmann, K. M. 1987 30–60 day atmospheric oscillations: composite life cycles of convection and circulation anomalies. *Mon. Weather Rev.* **115**, 1407–1436.

Lambeck, K. 1980 *The Earth's variable rotation*, pp. xi, 449. Cambridge University Press.

Lambert, S. J. 1988 A comparison of operational global analyses from the European Centre for Medium Range Weather Forecasts (ECMWF) and the National Meteorological Center (NMC). *Tellus* A **40**, 272–284.

Lange, A. & Tokkola, E. 1988 *Results of the WMO/CAS NWP data study and intercomparison project for forecasts for the northern hemisphere in 1987.* World Weather Watch Technical Report No. 6 of programme on short and medium range weather prediction research (PSMP), WMO TD – no. 270.

Langley, R. B., King, R. W. & Shapiro, I. I. 1981 Atmospheric angular momentum and the length of the day: a common fluctuation with a period near 50 days. *Nature Lond.* **294**, 730–733.

Legras, B. & Ghil, M. 1985 Persistent anomalies, blocking and variations in atmospheric predictability. *J. atmos. Sci.* **42**, 433–471.

Lindzen, R. S. 1965 On the asymmetric diurnal tide. *PAGEOPH* 142–147.

Longuet-Higgins, M. S. 1968 The eigenfunctions of Laplace's tidal equations over a sphere. *Phil. Trans. R. Soc. Lond.* A **262**, 511–607.

Lorenc, A. C. 1986 Analysis methods for numerical weather prediction. *Q. Jl R. met. Soc.* **112**, 1177–1194.

Madden, R. A. 1979 Observations of large-scale traveling Rossby waves. *Rev. Geophys. Space Phys.* **17**, 1935–1949.

Madden, R. A. 1986 Seasonal variations in the 40–50 day oscillation in the tropics. *J. atmos. Sci.* **43**, 3138–3158.

Madden, R. A. & Julian, P. R. 1972 Description of global-scale circulation cells in the tropics with 40–50 day period. *J. atmos. Sci.* **29**, 1109–1123.

PHILOSOPHICAL TRANSACTIONS OF THE ROYAL SOCIETY A MATHEMATICAL, PHYSICAL & ENGINEERING SCIENCES

Mason, B. J. 1986 Numerical weather prediction. *Proc. R. Soc. Lond.* A **407**, 51–60.

McFarlane, N. A. 1987 The effect of orographically excited gravity wave drag on the general circulation of the lower stratosphere and troposphere. *J. atmos. Sci.* **44**, 1775–1800.

Miller, M. J. 1988 *The sensitivity of systematic errors of the ECMWF global forecast model to parametrized processes.* WMO CAS/JSC WGNE Report No. 12, 289–296.

Miller, M. J., Palmer, T. N. & Swinbank, R. 1989 Parametrization and influence of subgrid scale orography on general circulation and numerical weather prediction models. *Meteorology atmos. Phys.* **40**, 84–109.

Milton, S. F. & Dickinson, A. 1988 *Systematic errors in 30 day integrations of the UKMO numerical weather prediction and climate models.* WMO CAS/JSC WGNE Report No. 12, 103–111. WMO TD No. 273.

Mitchum, G. T. & Lukas, R. 1987 The latitude–frequency structure of Pacific sea level variation. *J. phys. Oceanogr.* **17**, 2362–2365.

Morgan, P. J., King, R. W. & Shapiro, I. I. 1985 Length of day and atmospheric angular momentum: a comparison for 1981–1983. *J. geophys. Res.* **90**, 12,645–12,652.

Moritz, H. & Mueller, I. I. 1987 *Earth rotation: theory and observation*, pp. xx, 617. New York: Ungar.

Munk, W. H. & Macdonald, G. J. F. 1960 *The rotation of the Earth*, pp. xix, 323. Cambridge University Press.

Naito, I., Kikuchi, N. & Yokoyama, K. 1987 Results of estimating the effective atmospheric angular momentum functions based on the JMA global analysis data. *Publ. Int. Latitude Observatory of Mizusawa* **20** (1, 2), 1–11.

Nowlin, W. D. Jr & Klinck, J. M. 1986 The physics of the Antarctic circumpolar current. *Rev. Geophys.* **24**, 469–491.

Palmer, T. N., Shutts, G. J. & Swinbank, R. 1986 Alleviation of a systematic westerly bias in general circulation and numerical weather prediction models, through an orographic gravity wave parametrization. *Q. Jl R. met. Soc.* **112**, 1001–1039.

Reinhold, B. 1987 Weather régimes: the challenge in extended-range forecasting. *Science, Wash.* **235**, 437–441.

Risbey, J. S. & Stone, P. H. 1988 Observations of the 30–60 day oscillation in zonal mean atmospheric angular momentum and cloud cover. *J. atmos. Sci.* **45**, 2026–2038.

Rochester, M. G. 1984 Causes of fluctuations in the Earth's rotation. *Phil. Trans. R. Soc. Lond.* A **313**, 95–105.

Rosen, R. D. & Salstein, D. A. 1983 Variations in atmospheric angular momentum on global and regional scales and the length of the day. *J. geophys. Res.* **88**, 5451–5470.

Rosen, R. D. & Salstein, D. A. 1985 Contribution of stratospheric winds to annual and semi-annual fluctuations in atmospheric angular momentum and length of day. *J. geophys. Res.* **90**, 8033–8041.

Rosen, R. D., Salstein, D. A., Miller, A. J. & Arpe, K. 1987*a* Accuracy of atmospheric angular momentum estimates from operational analyses. *Mon. Weather Rev.* **115**, 1627–1639.

Rosen, R. D., Salstein, D. A., Nehrkorn, T., McCalla, M. R. P., Miller, A. J., Dickey, J. O., Eubanks, T. M. & Steppe, J. A. 1987*b* Medium range numerical forecasts of atmospheric angular momentum. *Mon. Weather Rev.* **115**, 2170–2175.

Sakellarides, G. 1989 *Atmospheric effective angular momentum functions for 1986–1987.* ECMWF Tech. Rep. 62.

Salstein, D. A. 1987 Operational production of effective (atmospheric) angular momentum functions for Earth rotation and polar motion. In *Bureau International de l'Heure, Annual Report for 1986.* Observatoire de Paris.

Shaw, D. B., Lönnberg, P., Hollingsworth, A. & Unden, P. 1987 Data assimilation: the 1984/85 revisions of the ECMWF mass and wind analysis. *Q. Jl R. met. Soc.* **113**, 533–566.

Simmons, A. J. & Burridge, D. M. 1981 An energy and angular-momentum conserving finite difference scheme and hybrid vertical coordinates. *Mon. Weather. Rev.* **109**, 758–766.

Simmons, A. J., Wallace, J. M. & Branstator, G. W. 1983 Barotropic wave propagation and instability and the atmospheric teleconnections pattern. *J. atmos. Sci.* **40**, 1363–1392.

PHILOSOPHICAL TRANSACTIONS OF THE ROYAL SOCIETY A MATHEMATICAL, PHYSICAL & ENGINEERING SCIENCES

Simmons, A. J., Burridge, D. M., Jarraud, M., Girard, C. & Wergen, W. 1989 The ECMWF medium range prediction models: development of the numerical formulations and the impact of increased resolution. *Meteorology atmos. Phys.* **40**, 28–60.

Spillane, M. C., Enfield, D. B. & Allen, J. S. 1987 Intraseasonal oscillation in sea level along the west coast of the Americas. *J. phys. Oceanogr.* **17**, 313–325.

Swinbank, R. 1985 The global atmospheric angular momentum balance inferred from analyses made during the FGGE. *Q. Jl R. met. Soc.* **111**, 977–992.

Tibaldi, S., Branković, C. & Cubasch, U. 1987 *30 day integrations using the operational ECMWF spectral model.*

Tibaldi, S., Palmer, T. N., Branković, C. & Cubasch, U. 1990 *Extended-range predictions with ECMWF models. Influence of horizontal resolution on systematic errors and forecast skill. Q. Jl R. met. Soc.* **116**, 835–866.

Tiedtke, M., Heckley, W. & Slingo, J. 1988 Tropical forecasting at ECMWF: the influence of physical parametrization on the mean structure of forecasts and analysis. *Q. Jl R. Soc.* **114**, 639–664.

Trenberth, K. E. & Christy, J. R. 1985 Global fluctuations in the distribution of atmospheric mass. *J. geophys. Res.* **90**, 8042–8052.

Trenberth, K. E. & Olsen, J. G. 1988 An evaluation and intercomparison of global analyses from the National Meteorological Center and the European Centre for Medium Range Weather Forecasts. *Bull. Am. Meteorology Soc.* **69**, 1047–1057.

Vautard, R., Legras, B. & Déqué, M. 1988 On the source of mid-latitude low-frequency variability. Part 1. A statistical approach to persistence. *J. atmos. Sci.* **45**, 2811–2843. Part 2. Non-linear equilibration of weather regimes. 2845–2867.

Vondrák, J. 1977 Problem of smoothing observational data II. *Bull. astr. Inst. Czech.* **28**, 84–89.

Vondrák, J. & Pejović, N. 1988 Atmospheric excitation of polar motion: comparison of the polar motion spectrum with spectra of effective atmospheric angular momentum functions. *Bull. astr. Inst. Czech.* **39**, 172–185.

Wahr, J. M. 1983 The effects of the atmosphere and the oceans on the Earth's wobble. II. Results. *Geophys. Jl R. astr. Soc.* **74**, 451–487.

Wahr, J. M. 1986 Geophysical aspects of polar motion, variations in the length of the day and the luni-solar nutations. In *Space geodesy and geodynamics*, (ed. A. J. Anderson & A. Cazenave), pp. 281–313. London: Academic Press. (x + 490 pages.)

Wahr, J. M. 1988 The Earth's rotation. *A. Rev. Earth planet. Sci.* **16**, 231–249.

Wahr, J. M. & Oort, A. H. 1984 Friction and mountain-torque estimates from global atmospheric data. *J. atmos. Sci.* **41**, 190–204.

Wallace, J. M., Tibaldi, S. & Simmons, A. J. 1983 Reduction of systematic forecast errors in the ECMWF model through the introduction of an envelope orography. *Q. Jl R. met. Soc.* **109**, 683–717.

Wang, B. 1988 Comments on 'an air–sea interaction model of intraseasonal oscillation in the tropics'. *J. atmos. Sci.* **45**, 3521–3525.

Wergen, W. 1989 Normal mode initialization and atmospheric tides. *Q. Jl R. met. Soc.* **115**, 535–545.

White, A. A. 1989 A relationship between energy and angular momentum conservation in dynamic models. *J. atmos. Sci.* **46**, 1855–1860.

Wilson, C. R. & Haubrich, R. A. 1976 Meteorological excitation of the Earth's wobble. *Geophys. Jl R. astr. Soc.* **46**, 707–744.

Wolf, W. L. & Smith, R. B. 1987 Length of day changes and mountain torque during El Niño. *J. atmos. Sci.* **44**, 3656–3660.

Wyrtki, K. 1985 Sea level fluctuations during the 1982–83 El Niño. *Geophys. Res. Lett.* **12**, 125–128.

Yoder, C. F., Williams, J. G. & Parke, M. E. 1981 Tidal variations of Earth rotation. *J. geophys. Res.* **86**, 881–891.

Received 8 February 1990; accepted 12 March 1990

PHILOSOPHICAL TRANSACTIONS OF THE ROYAL SOCIETY A MATHEMATICAL, PHYSICAL & ENGINEERING SCIENCES